Preparation of Ruthenium and Iridium Pincer-Type Pyridylidenes

by

Aristidis Pantelis Telly Athanasopoulos

A thesis

presented to the University of Waterloo

in fulfillment of the

thesis requirement for the degree of

Master of Science

in

Chemistry

Waterloo, Ontario, Canada, 2009

AUTHOR'S DECLARATION

I hereby declare that I am the sole author of this thesis. This is a true copy of the thesis, including any required final revisions, as accepted by my examiners.

I understand that my thesis may be made electronically available to the public.

Abstract

A new POCOP pincer-type ligand was synthesized and characterized. This new ligand gave rise to the first POCOP pyridylidene pincer-type ruthenium and iridium complexes. Investigations into structural and electronic parameters of these newly generated compounds were conducted. Furthermore, we prepared ruthenium dihydrogen and bis-dihydrogen complexes and studied them via deuterium labelling and low temperature NMR spectroscopy. These complexes were screened for catalysis in C-C coupling, C-H bond activation and ketone hydrogenation reactions.

Acknowledgements

At this time the author wishes to thank Professor Dmitri Goussev who has provided guidance and support as both an undergraduate and graduate supervisor. The time spent under his supervision provided an invaluable learning experience. The author would also like to that Professor Mike Chong and Professor Eric Fillion for taking the time to be on my committee.

Special thanks to my co-worker Brandon for his friendship and support in the lab. Lastly, I wish to acknowledge my family and friends for their continuous support throughout my undergraduate and graduate career.

Table of Contents

List of Abbreviations

AIBN	Azobisisobutyronitrile
Bu^t	*tert*-Butyl
COE	Cyclooctene
Cy	Cyclohexyl
Mes	Mesityl
NHC	N-heterocyclic carbene
Ph	Phenyl
POCOP	6-Methylpyridine-2,4-bis(di-*t*-butyl phosphinite)
^iPr	Isopropyl
tbe	*tert*-Butylethylene
TTMSS	Tris(trimethylsilyl)silane

1.0 Introduction

In our group, we deal with the fundamental problems of ligand design. We are interested in developing a series of strong electron donors: pyridine-based pincer carbenes. These ligands are expected to give rise to electron rich metal complexes which have a potential for several important applications in homogeneous catalysis.

1.1 N-heterocyclic carbenes

N-heterocyclic carbenes (NHCs) are becoming increasingly popular in organometallic chemistry and transition metal catalysis. Such ligands possess exceptional thermal stability and good electron donating properties. Wanzlick reported the first NHC in 1961.[1] Due to problems isolating the carbene and the lack of potential applications, NHCs remained relatively unexplored until 1991, when Arduengo et al. made an important breakthrough and reported the first stable crystalline carbene.[2] This breakthrough revived interest in the NHC type ligands which led to an exponential increase in the number of reports utilizing NHCs in transition metal chemistry. These ligands have demonstrated their utility in a variety of diverse catalytic processes including olefin metathesis and palladium-catalyzed coupling reactions.[3]

N-heterocyclic carbenes are good electron donors. They are somewhat analogous to tertiary phosphines, yet bind to metals more strongly and apparently surpass phosphines in electron donor strength. As a result, NHCs have replaced tertiary phosphines in a number of catalytic transformations. Typical NHCs are derivatives of imidazole, where the two nitrogen atoms are located adjacent to a central carbenic carbon at the C2 position. The nitrogen atoms play a dominant role in carbene stabilization, donating lone pair electron density into the formally empty p-orbital of the carbene

carbon. *N*-substituents can be varied to provide NHC compounds with steric stabilization and the desired steric environment. Furthermore, *N*-substituents play a key role in tuning the electronic properties of the ligand.[4] Common structures of NHCs are shown in Chart 1.

Chart 1

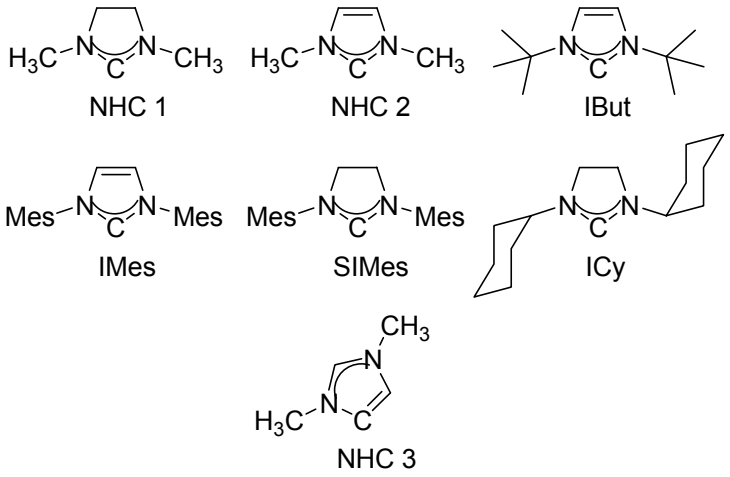

NHC type complexes are thermally stable making them very useful in catalysis. For example, ruthenium-NHC catalysts **1**[5] and **2**[6] (Chart 2) have allowed for the olefin metathesis production of carbocycles and heterocycles from acyclic diene precursors that were unattainable by classical Schrock and Grubbs catalysts **3**[7] and **4**[8]. Interestingly, bulky mesityl (Mes) substituents play a major role in the accelerated catalytic activity in NHC systems **1** and **2**. The strong steric pressure exerted by these NHC-ligands promotes olefin coordination, and lower the metathesis reaction barrier thereby accelerating reaction rates.[9]

Chart 2

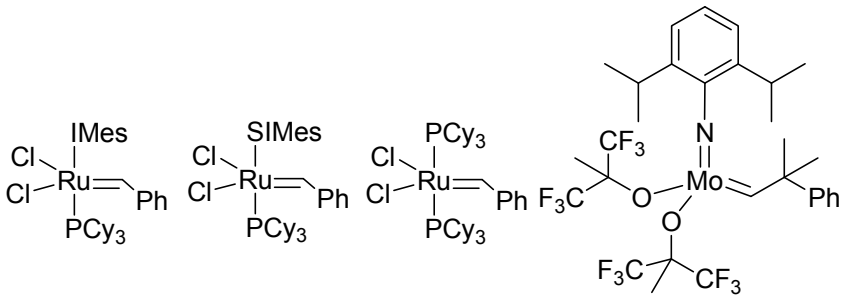

1 **2** **3** **4**

Recently, an 'abnormal' type of NHC was discovered by Crabtree et al.[10] It was named this way due to its unconventional binding mode to metals via the C4 carbon. Compared to normal NHCs, abnormal *N*-heterocyclic carbenes (aNHCs) offer different steric and electronic properties. Crabtree suggested that aNHCs are stronger electron donors than conventional NHCs. A representative model of an aNHC, **NHC3**, can be seen in Chart 1.

Infrared spectroscopy is an effective technique organometallic chemists use to measure the relative donor strength of ligands. The ligands are bound to metal carbonyl complexes and IR spectroscopy is used in determining the vibration frequency of the carbonyl C-O bond (ν(CO)). More electron donating ligands make metal centers more electron rich, resulting in stronger back donation into the empty p(π*) orbital of CO destabilizing the C-O bond. Hence, stronger donating ligands result in longer C-O bond lengths and lower ν(CO).

IR spectroscopy data collected by Crabtree gives estimates of the net electron donor power of aNHC **5**, normal NHC ligands **6a** and **6b** (Chart 3), as well as phosphine ligands, bound to the $Ir(CO)_2Cl$ fragment (Table 1).[4]

Chart 3

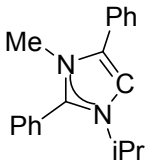

5

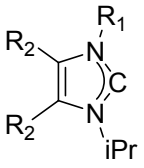

6a, b

a: R1 = Me, R2 = Ph
b: R1 = Ph, R2 = H

From Table 1 it is seen that conventional NHCs, **6a** and **6b**, have higher donor power than PEt_3, P^iPr_3 and even PCy_3, one of the most powerful donating phosphine ligands. In addition, CO stretching frequencies confirm that abnormally binding NHC **5**, demonstrates far greater donating power than normally bound NHCs **6a** and **6b**. This validates Crabtree's claim that aNHCs are stronger donors relative to NHCs.

Table 1. CO stretching frequencies in $IrCl(CO)_2L$ complex

L	$\nu_{av}(CO)$ (cm^{-1})
5	2003
6a	2017
6b	2019
PCy_3	2028
P^iPr_3	2032
PEt_3	2038

1.2 Pyridine-based carbenes

Pyridine is an integral component of our proposed research project. There is a clear relationship between the 6-electron π-systems of pyridine and imidazole. Three 'abnormal' carbenes can be derived from pyridine (**PyC2**, **PyC3**, **PyC4**) in the same way as C2 and C4 type NHCs can be derived from imidazole. Scheme 1 exhibits the carbene derivatives of imidazole and pyridine systems.

Scheme 1

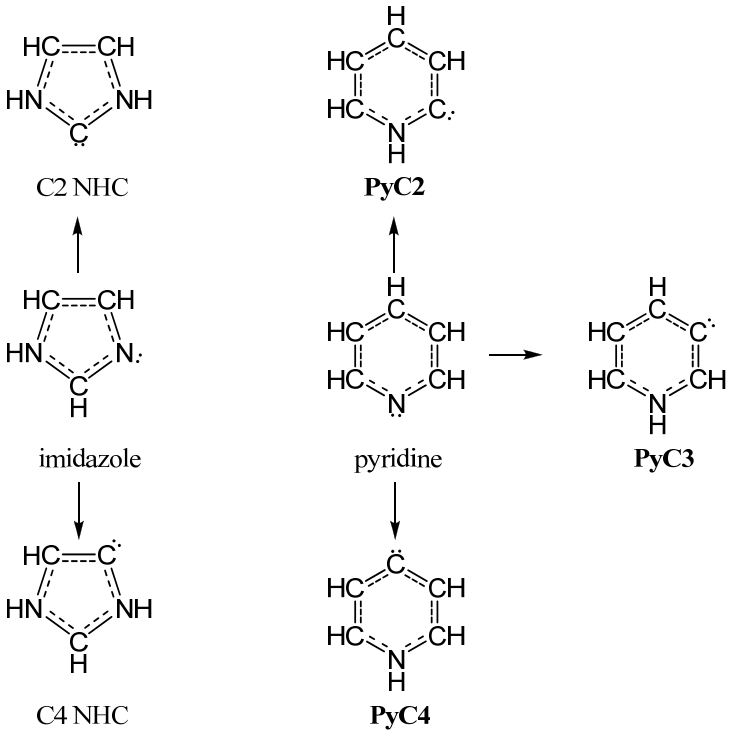

N-heterocyclic carbenes derived from pyridine can be expected to exhibit σ-donor and π-acceptor properties similar to those of aNHC ligands. This becomes apparent when we consider the resonance structures in Chart 4.

Chart 4

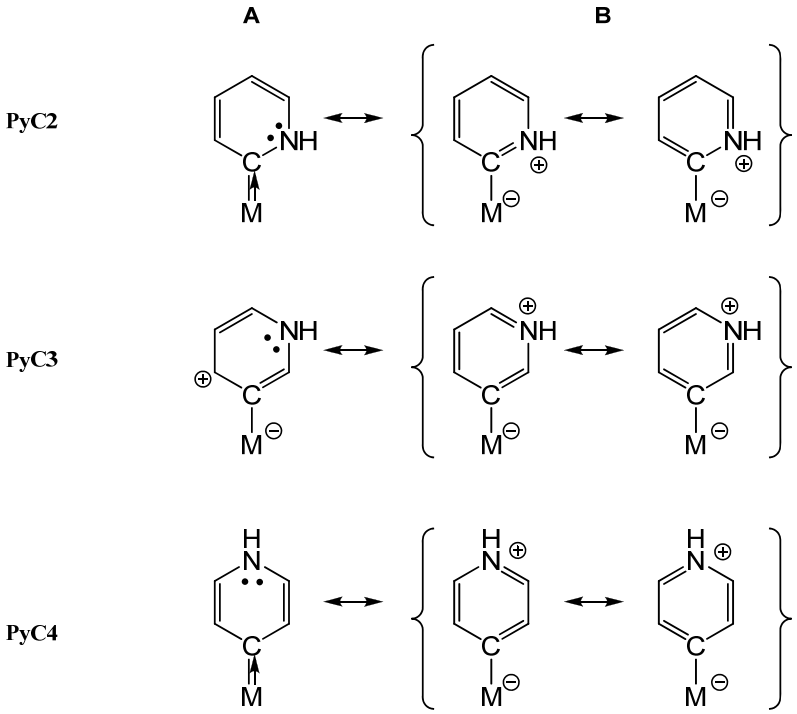

From a qualitative perspective, we expect that pyridine based carbenes are exceptional donor ligands largely due to the ionic nature of their resonance structures. In all cases, we see a full electron transfered from ligand to the metal center, indicating strong electron-donor character of the PyC system (form **B)**. Neutral resonance structures of **PyC2** and **PyC4** suggest some possible π-acceptor properties (form **A**). It is noteworthy that **PyC3** is without any neutral structure and it can be more strongly donating than **PyC2** and **PyC4**.

There are several examples of PyC type complexes found in the literature. Structures relevant to this research project are illustrated in Chart 5.

Chart 5

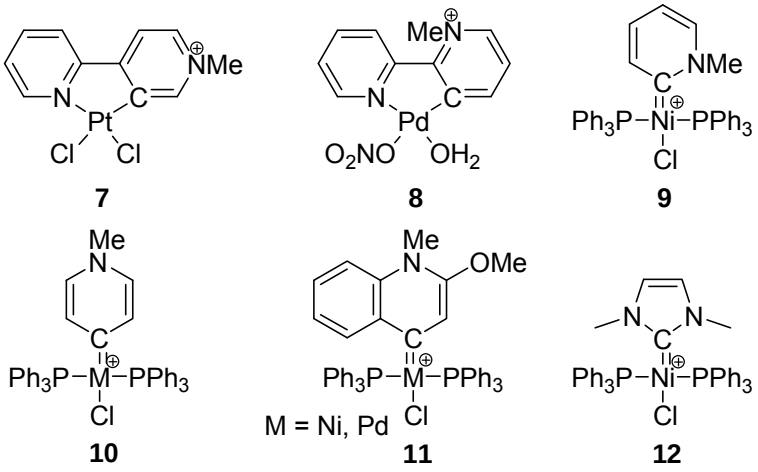

Structures **7**[11] and **8**[12] are analogous to the PyC3 ligand system while structures **9** and **10** are compounds based on the PyC2 and PyC4 ligand makeup. The carbene ligand in complex **11** is derived from quinoline and it is related to the PyC4 framework. The carbene carbon atoms in the nickel complexes **9**, **10** and **11** resonate at δ ^{13}C values 205.3, 193.5 and 215.3 ppm, respectively, in the region that would indicate a carbene carbon (~ 200+ ppm).[13] These values are significantly downshifted compared to those of conventional NHC **12**, which resonates at 158.6 ppm.[14]

We can determine the major resonance contributions of the PyC ring systems in Chart 5 by examining C-C bond distances. In the PyC3 ligand systems of **7** and **8**, similar C-C bond distances are observed in the PyC ring, indicating dominant resonance contributions of form **B**. Conversely in **9**, there are short C-C bond distances of 1.37 Å and 1.36 Å for C3-C4 and C5-C6, while a longer bond distance of 1.43 Å is observed for the C2-C3 bond. Similarly, in the nickel complex **10**, short C2-C3 and C5-C6 bond distances of 1.35 Å and 1.36 Å, and longer C3-C4 and C4-C5 bond distances of greater than 1.40 Å are observed. The C-C bond distances in compounds **9** and **10**, are indicative of dominant resonance contributions from carbenes of form **A**.

Our group used DFT to calculate CO stretching frequencies of the carbonyl complexes $Ni(CO)_3L$ to evaluate donor properties of PyC2, PyC3, and PyC4, and compare these ligands with *N*-heterocyclic carbenes and several important phosphine ligands. It is clear from the computational data in Chart 6 that the pyridylidene ligands are exceptionally good electron donors toward the $Ni(CO)_3$ fragment. It is noteworthy that the calculated and experimental νCO values are consistent.

Chart 6

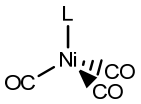

L =	**PyC3**	NHC-3	**PyC4**	**PyC2**	NHC-2	PBu^t_3	PPr^i_3	PMe_3	PPh_3
	← increasing donor ability								
ν_{CO} (A_1), cm^{-1} =	2042.5	2043.1	2044.9	2053.2	2053.9	2055.3	2059.2	2065.2	2067.5
Known experimental values:						2056.1	2059.2	2064.1	2068.9

1.3 Pincer Ligated Complexes

Pincer ligand systems are an effective means of tuning the properties of transition metal complexes to maximize the efficiency of catalytic reactions. Pincer ligands are named after the manner in which they bind to metals. They are tridentate ligands flanking metal centers with *trans*-positioned donor groups **D**. Conventional pincer ligands feature an arene backbone. Donor groups, in the 'arms' of the ligand can be varied to offer useful steric and electronic properties. Furthermore, **Y** groups can be modified to influence the electronic parameters of the ligand. For example donor groups (Y = NR or O) should generate more electron rich π-systems and as a result give rise to more electron rich complexes. Remote electronic modifications can be obtained by varying the **R** group anchored to the backbone of the ligand. A general form for a pincer complex is illustrated in Chart 7.[15]

Chart 7

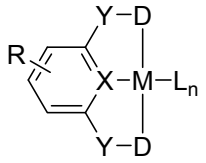

D = NR_2, PR_2, $P(OR)_2$
Y = CH_2, NH, O, carbonyl
X = C, N
R = H, alkyl, aryl

Generally in organometallic chemistry ligand names are shortened to several descriptive characters. In pincer-type complexes, the characters typically correspond to the atoms bonded directly to the metal center, and in some cases incorporating Y groups into the shortened form as well. For example, the abbreviated name given for the general form in Chart 7 would be DXD or DYXYD. Pincer ligands will be described in this manner throughout this research project.

1.4 Pincer Complexes in Catalysis

Alkane dehydrogenation is an extremely attractive area of research owing to the possibility of generating valuable alkenes as major organic feedstock. A major breakthrough came in 1996 when Jensen et al. successfully catalyzed the transfer dehydrogenation reaction of an alkane with the iridium pincer complex, $[IrH_2(PCP)]$ where PCP = $[C_6H_3\text{-}2,6\text{-}(CH_2P(Bu^t)_2)_2]$ (Chart 8).[16]

Chart 8

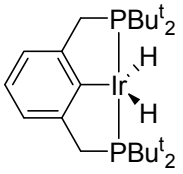

To date, the most active catalysts for transfer dehydrogenation belong to the family of iridium dihydrido pincer complexes. In transfer dehydrogenation, an alkane substrate is dehydrogenated by an iridium pincer-ligated catalyst in the presence of a sacrificial alkene, typically *tert*-butylethylene (tbe), at 200 °C (Scheme 2). For the

commonly used benchmark reaction, cyclooctane has been the standard substrate due to its low enthalpy of dehydrogenation (23.3 kcal/mol). An acceptor alkene reduces the $[Ir(H)_4(PCP)]$ intermediate back to the unsaturated $[Ir(H_2)(PCP)]$, thus regenerating the catalyst.

Scheme 2

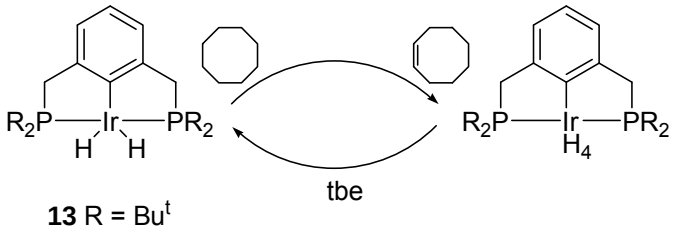

13 R = Bu^t

Iridium pincer complexes of this type are highly robust and can withstand high temperature reaction conditions making them well suited for transfer dehydrogenation of alkanes. Turnover numbers (TONs) as high as 1000 have been reported with compound **13**.[17]

Recently, Brookhart and coworkers prepared a series of supported iridium(POCOP) complexes (Chart 9). Upon dehydrochlorination of these compounds, they become catalytically active for transfer dehydrogenation. They achieved unprecedented TONs between 1400 and 2200 and turnover frequencies (TOFs) between 1.6 and 2.4 s^{-1}, at 200 °C.[18]

Chart 9

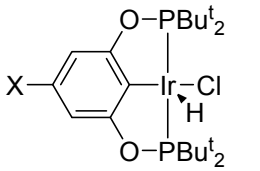

X = MeO, Me, H, F, C_6F_5

Acceptorless alkane dehydrogenation occurs without the use of a sacrificial olefin and is potentially more significant. It has been investigated using cyclodecane due to its

high boiling point (201 °C). It is conducted in an open system and involves the liberation of H_2 from the iridium catalyst via vigorous refluxing of the solution (Scheme 3). Goldman and Liu demonstrated how the steric environment at the phosphorus groups can be very influential in the activity of the catalyst. Interestingly, the bulky *tert*-butyl groups in **13** inhibit H_2 addition. Complex **14** contains medium size isopropyl phosphine donor groups and as a result contains less steric congestion at the metal center. The metal is now more available for substrate ligands and consequently **14** was far more active, yielding turnover rates a full order of magnitude greater than **13**.[19]

Scheme 3

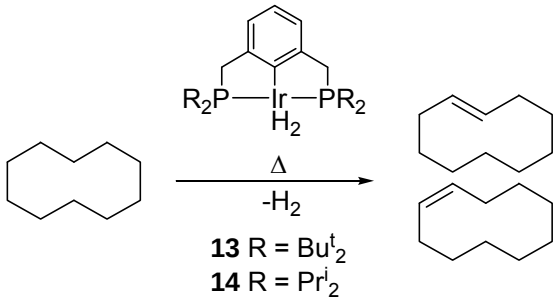

A recent investigation by Goldman and Brookhart[20] has lead to an interesting application of alkane dehydrogenation catalysis in the production of synthetic liquid fuels (eg. Diesel fuels *n*-alkanes ranging from ~C_9 to C_{20}) through tandem alkane dehydrogenation-olefin metathesis reactions of shorter chain *n*-alkanes. Scheme 4 outlines the basic alkane dehydrogenation-olefin metathesis tadem reaction, where a dehydrogenation catalyst, M, reacts with short chain alkanes to give their cooresponding terminal alkenes. In turn, an internal alkene and ethylene are generated through olefin metathesis of 1-alkenes, followed by hydrogenation with MH_2 yielding two new alkanes and regenerating the catalyst M.

Scheme 4

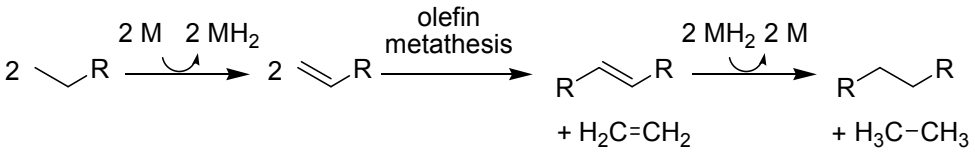

Tandem systems developed by Goldman and Brookhart comprised of PCP **15 a, b**, POCOP **16** pincer-type dehydrogenation catalysts, and Schrock-type metathesis catalyst **17** (Chart 10). Early experiments employed *n*-hexane as the substrate, anticipating that dehydrogenation-olefin metathesis-hydrogenation, would produce *n*-decane and ethane. However, the product distribution was concentrated in the C_2 to C_5 and C_7 to C_{10} ranges. Pincer-type complexes **15 a, b** and **16**, dehydrogenate with high selectivity towards the formation of α-olefins. Thus, olefin isomerization before olefin metathesis was likely responsible for diverging product distribution. Interestingly, the Schrock-type catalyst limited product formation as it underwent decomposition under dehydrogenation conditions (125 °C in sealed glass vessel). However, the pincer-type complexes were very robust and no evidence of catalyst decomposition was observed.

Chart 10

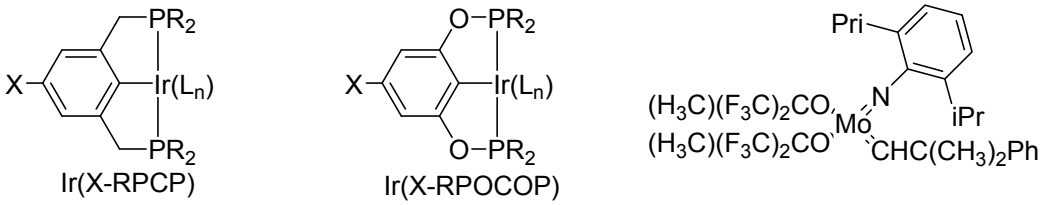

15a: R = Bu^t, X = H
15b: R = Pr^i, X = OMe
L= H_2 and/or H_4

16: R = Bu^t, X = H
L= C_2H_4, H_2

17

Synthetic fuels will become increasingly more attractive as world supplies of liquid hydrocarbon diminish. Tandem dehydrogenation-olefin metathesis systems offer a step towards breaking our dependence on hydrocarbons from sources of oil.

Milstein and coworkers have recently reported a dearomatized pyridine based ruthenium pincer complex, **18** (Scheme 5). Interestingly, this catalyst facilitates important organic transformation including reversible hydrogenation/dehydrogenation and coupling reactions. Primary alcohols can be oxidized to give aldehydes and then esters, while secondary alcohols to give ketones under dehydrogenation conditions. Amides are formed from alcohols and amines, thus avoiding the use of acid chlorides and anhydrides which often produce harmful waste. Additionally, molecular hydrogen is produced as a byproduct. Also, the reactions are reversible under H_2, thus avoiding the use of stoichiometric amounts of metal hydride reagents.[21]

Scheme 5

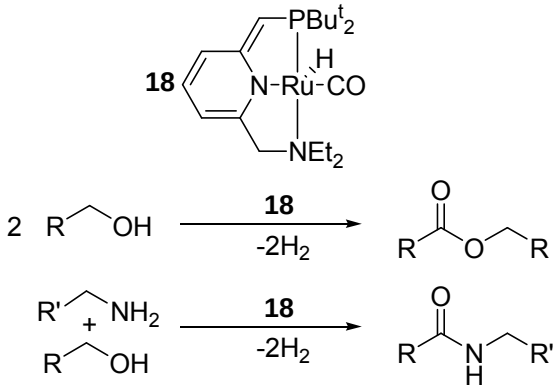

Pincer complexes have demonstrated great potential for catalytic applications involving activation, cleavage and formation of σ-bonds. This brief survey of current literature explains our interest in developing new pincer-type ligands.

2.0 Proposed Research

Well defined pincer ligand systems are useful for controlling the properties of transition metal centers. We would like to develop a series of new type of pyridylidene pincer ligand and study structural and electronic properties of their corresponding metal complexes. The following section outlines proposed research which consists of five sections devoted to (i) ligand design, (ii) ligand synthesis, (iii) alkylation, (iv) metalation, and (v) catalysis.

2.1 Ligand design

We are interested in synthesizing a series of pyridylidene pincer-type ligands as illustrated in Chart 11. Pyridine-based pincer ligands of this type are new compounds, and while related compounds have been reported, none of which feature a carbenic C-M bond.

Chart 11

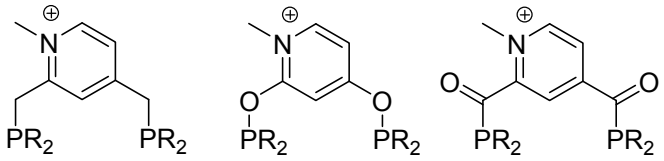

Upon observation of ligands **PCP**, **POCOP**, and **PCP^{CO}**, differences in the 'arms' at the 2,4-position on pyridine are evident. A methylene linkage is present in PCP ligand, a phosphinite linkage is present in POCOP, and a carbonyl linkage is present in PCP^{CO}. These slight variations in ligand parameters will influence the structural and electronic properties of their corresponding metal complexes in very different ways.

We expect electron rich complexes formed with POCOP ligand. This can be attributed to π-electron donation into pyridine through oxygen atoms in the phosphinite

linkage. An opposite trend should be observed in complexes containing PCP^{CO} due to electron withdrawing effect by the carbonyl groups bonded to pyridine (Chart 12).

Chart 12

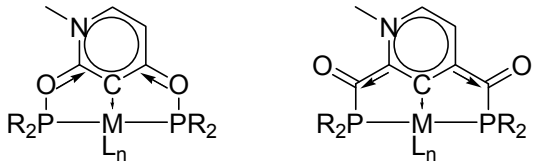

$[ML_n(POCOP)]$ $[ML_n(PCP^{CO})]$

The ligands proposed in this series should generate complexes with structural differences. For example, pyridine-oxygen and oxygen-phosphorus bond distances in POCOP complexes should be relatively short when compared to the methylene linkage bond distances present in PCP complexes. As a result, the bulky phosphorus donor groups in POCOP would be pulled back towards the ligand, away from the metal center. This would have significant impact on catalysis, as cavities for metal-substrate binding would be more available (Chart 13).

Chart 13

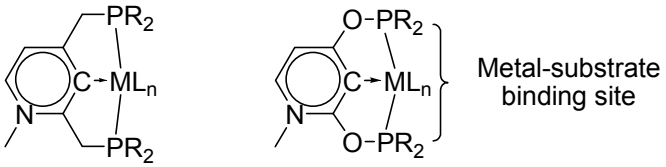

$[ML_n(PCP)]$ $[ML_n(POCOP)]$

Complex stability is another parameter that must be considered when designing new ligands. Generally, heating is employed during catalysis, thus complexes facilitating these reactions must be very robust. Pincer complexes are known for there durability, however they are still susceptible to decomposition at high temperature. The methylene linkage in PCP complexes is susceptible to decomposition at high temperatures through

intramolecular C-H bond activation. POCOP complexes should be more durable in this respect.

The 'arms' of the ligands will be located at the 2,4-position on the pyridine ring, giving way to a PyC3 conformation upon metalation. These ligands should produce electron rich metals due to the strong donor character of the PyC3 system. Referring back to the resonance forms **A** and **B** in Chart 4, for PyC3 there is a full one electron transfer from ligand to metal center in all resonance forms. We can expect the same kind of resonance contributions from **PCP**, **POCOP**, and **PCP^{CO}** ligands.

In addition, we believed that it was important to alkylate nitrogen in the pyridine backbone of the ligand, and there was a two-fold reason:

a) Alkylated nitrogen is necessary in obtaining carbene conformation upon metalation of the ligand. (refer to PyC3 resonance structures in Chart 4)
b) Alkylated nitrogen will block any undesirable coordination modes during metalation.

Lastly, bulky *tert*-butyl or medium size isopropyl phosphorus groups will be employed as donor groups for these ligands. The varying size should offer further tuning of the metal center steric environment.

2.2 Ligand synthesis

This section of the proposed research is devoted to ligand synthesis and will outline the synthetic steps necessary for obtaining this family of compounds. They will be produced in approximately 3-6 g quantities. Synthesis of these ligands will be achieved using the appropriate functionalized pyridine precursor. Through modification of these functional groups, we can add donor phosphorus groups at the ortho-para positions.

Trimethyloxonium tetrafluoroborate (Me_3OBF_4) will be utilized as the standard alkylating agent because we would like to avoid any halogen scrambling in our complexes which can be observed when using conventional alkyl halide alkylating agents. Due to the availability of three nucleophilic sites, one at nitrogen and two at phosphorus, potential problems could arise during *N*-alkylation. Different alkylation strategies will be discussed in Section 2.3.

The ligand precursor for POCOP is 2,4-dihydroxypyridine and is commercially available. POCOP can be obtained from a one step reaction involving a secondary chlorophosphine, PR_2Cl and the pyridine diol **19** in the presence of base. Triethylamine (NEt_3) will likely be our base of choice because it can be used in excess with any unreacted base easily removed through evaporation. Synthesis of *tert*-butyl and isopropyl phosphinites of **20** can be prepared utilizing $ClPBu^t_2$ and $ClPPr^i_2$ respectively, which are both commercially available. Scheme 6 outlines the synthesis.

Scheme 6

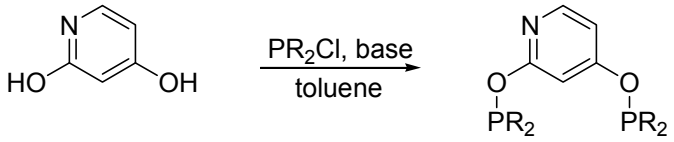

19 **20**

2,4-Pyridinedicarboxylic acid **21** is commercially available and will serve as the precursor for both PCP and PCP^{CO}. The dicarboxylic acid will be converted to 2,4-pyridine(biscarbonylchloride) **22** using thionyl chloride ($SOCl_2$). Two equivalents of HCl are produced in this reaction, with likely formation of a pyridinium salt. Thus, subsequent addition of base will be required. Compound **23** can be synthesized via reaction of acid

chloride **22** and secondary phosphine, HPR_2, in the presence of base. The synthesis of **23** is outline in Scheme 7.

Scheme 7

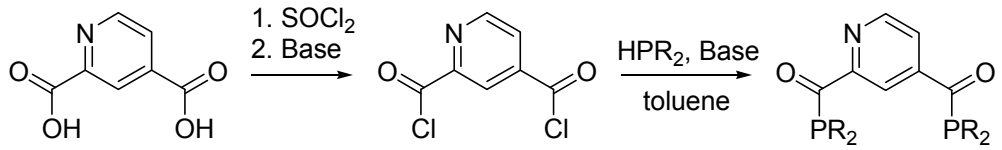

21 **22** **23**

The preparation of **24** from **23** presents one of the key synthetic challenges we will face. Our objective is to cleanly reduce the carbonyl compound **23** to its methylene equivalent **24** using a strong reducing agent such as lithium aluminum hydride ($LiAlH_4$). We expect that the reduction will work in much of the same way as amide reduction to their corresponding amines. The proposed synthesis of **24** is outlined in Scheme 8.

Scheme 8

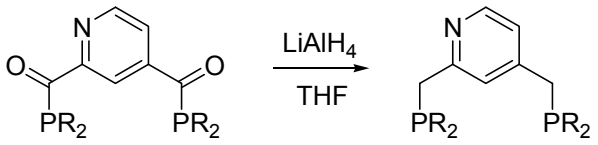

23 **24**

2.3 Alkylation

It is important that we find a general method of facilitating selective *N*-alkylation for all of the ligands studied. Our goal is to achieve clean and selective alkylation at nitrogen, while avoiding *P*-alkylation. Thus, phosphorus protection/deprotection will be explored for ligand alkylation. We will be investigating the use of boranes and chalcogens as phosphorus protecting agents.

Boranes are Lewis acids which readily form complexes with nucleophiles such as phosphorus. We will utilize boranes as protecting agents for the phosphorus donor

groups. Once we achieve selective borane protected phosphorus (eg. **25**), alkylation at nitrogen can be carried out. The general borane protection followed by alkylation reactions are illustrated in Scheme 9.

Scheme 9

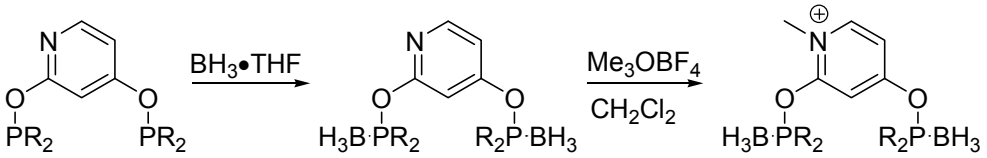

20 **25** **26**

We will explore the use of several different types of borane reagents for phosphorus protection. The simplest borane BH_3 has been employed in the literature as an effective phosphine protecting agent and will serve as a suitable starting point.[22] However, nitrogen is available to borane and will compete with phosphorus for complex formation. Therfore bulkier boranes, such as BEt_3 or BPh_3, will be considered for protection if poor selectivity becomes a problem. Once we have achieved *P*-protection, *N*-alkylation can be carried out using the standard alkylating agent. Lastly, strong Lewis bases such as amines, are typically employed in borane removal. We may explore mild nucleophilic solvents, such as methanol, as an alternative to amines.

In the literature, chalcogens have been utilized as phosphorus protecting groups (R_3P=X, X = O, S, Se).[23] This approach is very attractive as it is a facile and selective method of protecting phosphorus in our ligand series. Scheme 10 illustrates the general process utilizing sulfide and selenide protection for the preparation of the alkylated species **28**.

Scheme 10

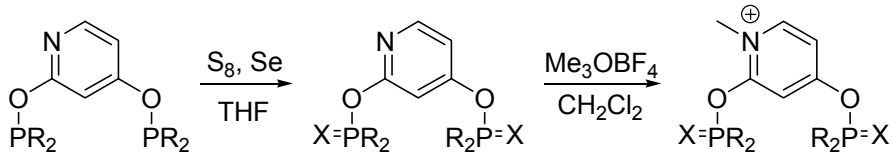

Phosphorus can be protected as a phosphine oxide, which can be easily obtained using oxidants such as hydrogen peroxide. Once phosphorus protection has been achieved, alkylation can then be carried out as illustrated in Scheme 11. There are two methods that will be considered for phosphine deprotection: Raney Nickel or silane reduction.

Scheme 11

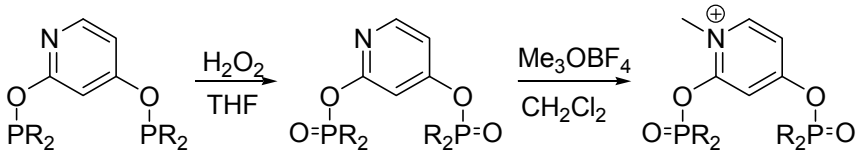

There are several examples in the literature where Raney Ni is utilized for the reduction of chalcogen-phosphorus bonds. However, heterogeneous Ni reductions of this type were reported as being slow. Also, large excesses of Ni were required.[24]

Phosphorus deprotection via silane reduction is an attractive alternative to Ni. It is a radical based reduction and takes place under free radical conditions. Azobisisobutyronitrile (AIBN) will be employed as the radical initiator. The reduction of phosphine-chalcogens is illustrated in Scheme 12. Chatgilialoglu and coworkers reported the reduction of phosphine sulfides and selenides by $(Me_3Si)_3SiH$. Interestingly, the reduction took place under mild conditions, with excellent yields (>90%) and fast

reaction rates (<6 h). We will explore the use of several silanes for phosphorus deprotection such as triethylsilane and tris(trimethylsilyl)silane.[25]

Scheme 12

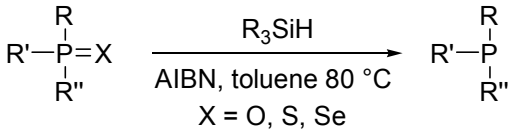

2.4 Metalation

The third component of this research project involves the preparation of late transition metal pincer complexes. Metals targeted for research are Ru, Os, Rh, Ir. Chloride complexes will be prepared for all of the proposed ligands in Chart 11. Metalation will be achieved by thermal cyclometalation and C-H bond activation reaction, using precursors $[RuCl_2(p\text{-cymene})]_2$ and $[MCl(COE)_2]_2$ (M = Rh, Ir) (Scheme 13). Osmium complexes will be synthesized from the metal precursor $[OsCl_6](NEt_4)_2$ in alcohols, under H_2 (Scheme 14).

Scheme 13

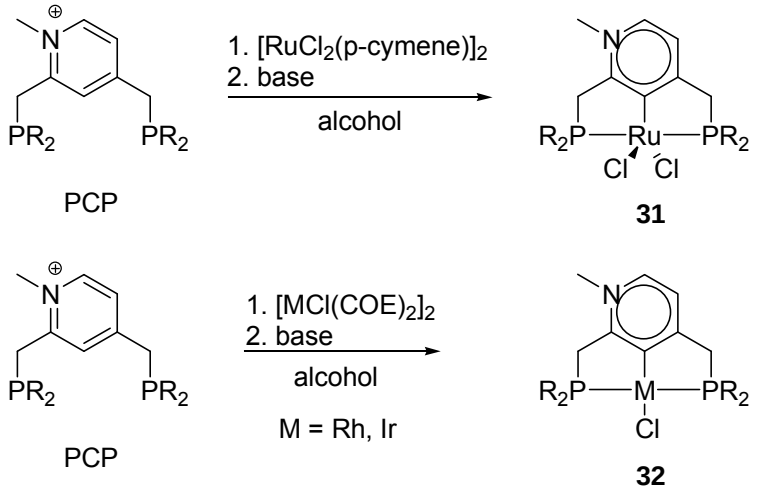

Scheme 14

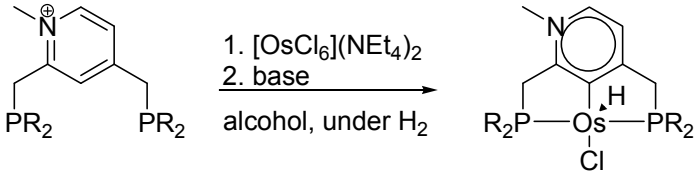

PCP **33**

The 16-electron compounds **31**, **32** and **33**, are Ru (II), M (I) (M = Rh, Ir) and Os (II) respectively. They will serve as suitable starting materials for a variety of hydridic species such as: RuHCl[PCP], MH_3Cl[PCP], MH_4[PCP] or MH_2[PCP] (M = Ru, Os), MH[PCP] and $MH_2[PCP]^+$ (M = Rh, Ir). Analogous compounds will be prepared with the cyclometalated ligands POCOP and PCP^{CO}.

Additionally, we will be attempting to isolate 14-electron species, such as M[PCP] (M = Ru, Os, Rh^+, Ir^+). Such coordinatively unsaturated compounds can be prepared by:

(a) thermal dehydrogenation, e.g. $IrH_2[PCP]^+ \rightarrow Ir[PCP]^+ + H_2$

(b) via transfer dehydrogenation, e.g. RuH_2[PCP] + *t*-$BuCH{=}CH_2$ → Ru[PCP] + *t*-$BuCH_2CH_3$

(c) by dehydrochlorination, e.g. OsHCl[PCP] + *t*-BuOK → Os[PCP] + KCl + *t*-BuOH

These 14-electron compounds should be useful for catalysis involving activation and bond cleavage of strong σ-bonds (C-H, N-H). The isolation of these compounds should be very challenging. Although rare, examples of 14-electron pincer complexes of ruthenium have been reported.[26]

2.5 Catalysis

We are going to synthesize exceptionally powerful electron donor ligands: pincer-type carbenes. These ligands and their complexes show promise towards activation and

cleavage of strong σ-bonds (C-H, N-H), especially the 14-electron species M[PCP], M[PCP^{CO}], and M[POCOP].

Acceptor/acceptorless alkane dehydrogenation will be screened with the metal hydride complexes MH_2[PCP] (M = Ru, Os) and $MH_2[PCP]^+$ (M = Rh, Ir), using the benchmark dehydrogenation of cyclooctane reaction. The iridium PCP pincer complexes mentioned in section 1.4 have been effective for catalytic alkane dehydrogenation. These classical pincer ligands are formally 5-electron donors, while the proposed pyridine-based pincer ligands are formally 6-electron donor ligands (Chart 14). Thus, it will be interesting to see if we can obtain catalytically active species of group 8 metals, ruthenium and osmium. Furthermore, ruthenium and osmium pincer complexes have not been investigated for alkane dehydrogenation.

Chart 14

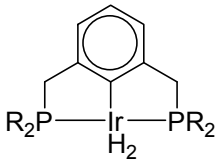

PCP ligand 5-electron donor

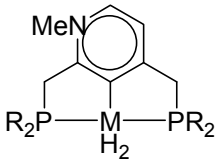

PCP ligand 6-electron donor

M = Ru, Os, Ir^+, Rh^+

Brookhart's series of iridium bis(phosphinite) complexes were found to be most active in transfer dehydrogenation of alkanes. Therefore, it will be particularly interesting exploring the activity of the related compounds MH_2[POCOP] (M = Ru, Os, Ir^+, Rh^+) (Chart 15).

Chart 15

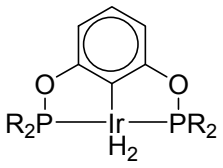

Brookhart's POCOP system

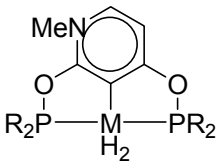

Pyridylidene POCOP system
M = Ru, Os, Ir^+, Rh^+

Milstein's pyridine-based pincer ligands are closely related to the proposed pyrdylidene pincer-type ligand. Both ligands contain a pyridine backbone; however Milstein's ligands bind to metals through a central nitrogen donor, where our proposed ligands contain a central carbene-metal bond. Nevertheless, these ligands are isoelectronic and strong electron donors. It will be interesting if we encounter a dearomatized PCP pincer complex analogous to Milstein's PNP and PNN complexes.

3.0 Results and Discussion

3.1 Investigation into POCOP Complexes

This section gives a brief summary of the key challenges we faced while working towards the preparation of POCOP and PCP complexes.

3.1.1 Preparation of POCOP Ligand

The POCOP ligand **34** was prepared via reaction of diol **19** with 2.3 equivalents of di-(*tert*-butyl)chlorophosphine and 3 equivalents of triethylamine in propionitrile (Scheme 15). The reaction mixture was heated to 90 °C over 20 h. Afterwards, the product was cooled to room temperature, filtered, and propionitrile removed under vacuum yielding a pale yellow solid. Then the product was extracted from the solid in diethyl ether followed by evaporation of the solvent yielding 97 % of the product as a pale yellow solid.

Scheme 15

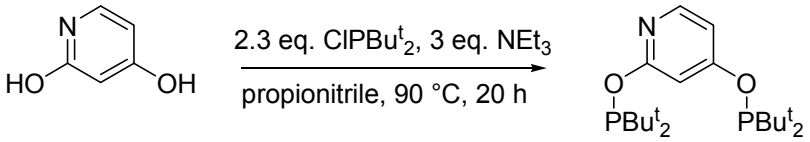

19 **34**

97 %

3.1.2 POCOP Metalation

Next, we wished to synthesize a ruthenium pincer complex from the pre-ligand **34**. An NMR tube reaction was prepared containing **34** and the ruthenium precursor $RuCl_2(PPh_3)_3$ and refluxed for 20 h. We expected formation of a tridentate pincer complex **35** via cyclometalation reaction. Unfortunately, ^{31}P NMR showed no evidence for the formation of **35**. Instead, ligand **34** formed a stable, five coordinate bidentate complex **36**, binding to ruthenium through nitrogen and one of the phosphorus groups.

Additional heating did not result in formation of **35** and clearly alkylation of nitrogen was necessary to eliminate it from participating in metalation.

Scheme 16

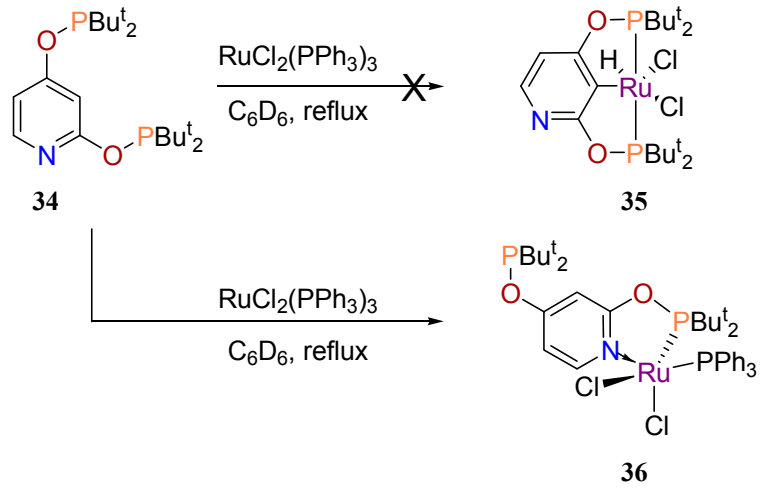

3.1.3 POCOP Protection

As mentioned previously in Section 2.3, pre-ligand **34** must be protected before alkylation can be achieved. Thus, we prepared a series of phosphinites protected as chalcogenides **37**, **38**, **39** and as a borane compound **40**(Scheme 17).

Scheme 17

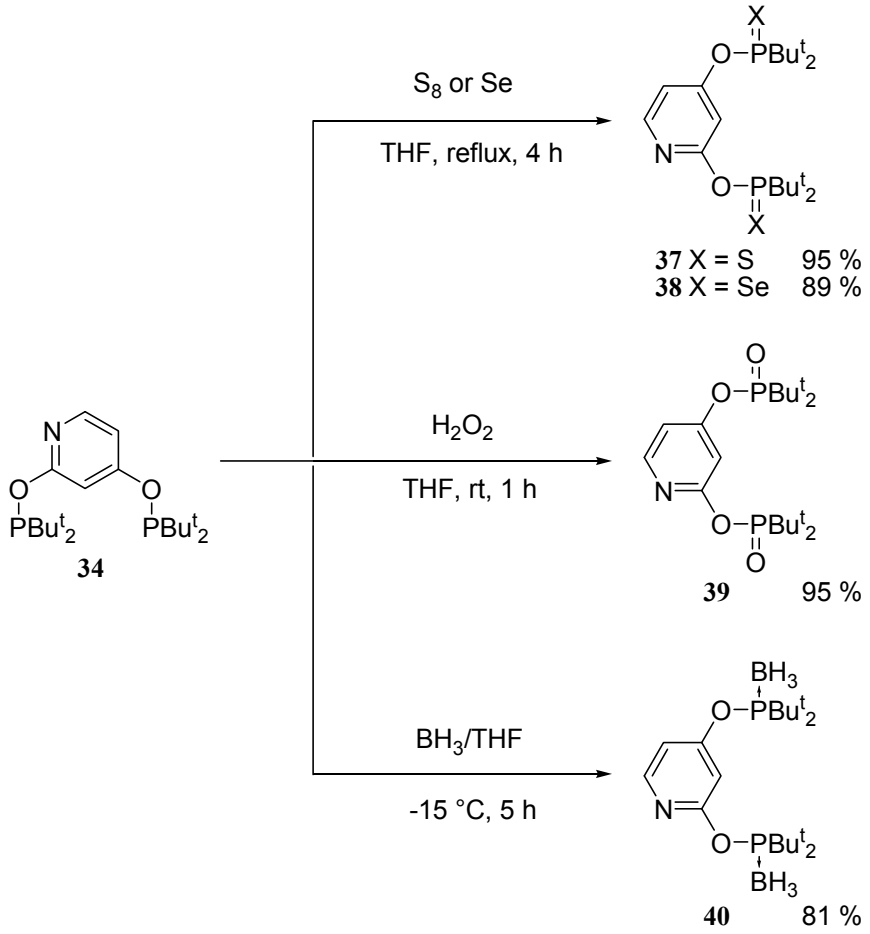

Initially we prepared sulfide **37** by reaction of **34** with S_8 in THF and refluxed for 4 h. Afterwards, THF was evaporated yielding 95 % of **37** as a pale yellow solid. Similarly, selenide **38** was produced under the same reaction conditions yielding 89 % of the product as a white solid. Furthermore, we synthesized an oxidized phosphinite **39** by reaction of **34** with H_2O_2 in THF. Once THF was evaporated, **39** was obtained in 95 % yield as a white solid.

Borane **40** was prepared via reaction of **34** with a 1 M solution of BH_3/THF complex. Once the reagents were combined, the reaction mixture was placed in a freezer for 5 h. The solvent was removed and product dried under vacuum yielding 81 % of **40** as a pale yellow solid.

3.1.4 POCOP Alkylation

Following phosphinite protection, our next challenge involved alkylation of compounds **37** – **40**. Alkylation of **37**, **39**, and **40** with Me_3OBF_4 was very straightforward as we achieved yields 86 % and above (Scheme 18).

Scheme 18

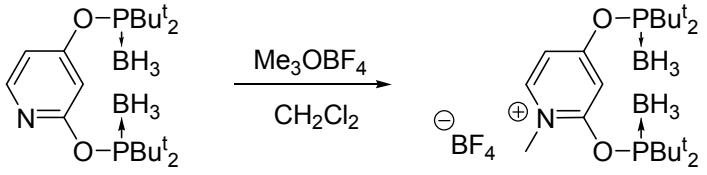

40 **41** 98 %

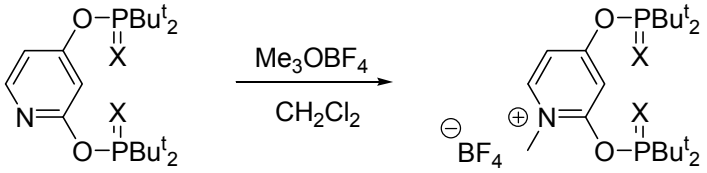

37 X = S
39 X = O

42 X = S 98 %
43 X = O 86 %

Unfortunately, we were unable to selectively alkylate selenide **38**. From NMR analysis, we observed a mixture of compounds containing alkylated nitrogen **44** and alkylated selenium compound **45** (Scheme 19). Due to the lack of selectivity for alkylation of **38**, we abandoned selenium as a protecting group.

Scheme 19

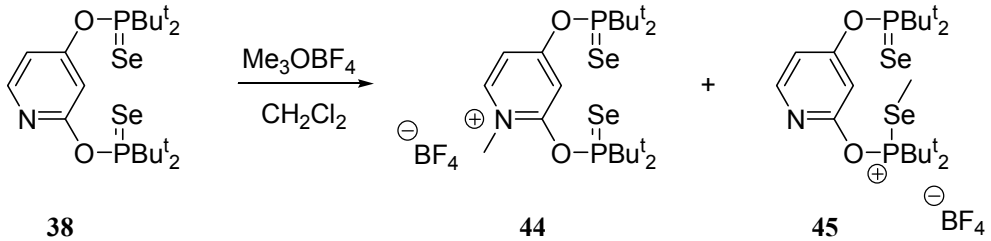

38 **44** **45**

3.1.5 POCOP Deprotection

Next we attempted deprotection of the alkylated compounds **41** – **43**. Decomplexation of borane compounds such as **41** classically involve the use of competitor Lewis bases. Thus, we utilized nitrogen bases such as *N*-methylmorpholine and triethylamine (Scheme 20). Unfortunately, the deprotection reactions proceeded with decomposition and afforded complicated mixtures according to ^{31}P NMR. Furthermore, we observed formation of di(tert-butyl)phosphine oxide **46** which was indicative of decomposition of the phosphinite linkage in **41**.

Scheme 20

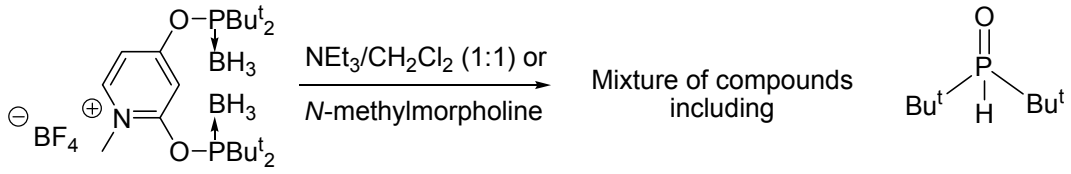

41 **46**

Similarly, we were unsuccessful in deprotecting **42** and **43**. For sulfide deprotection, we attempted Raney nickel reduction. However, the reduction was extremely slow and did not go to completion. Silane reduction on oxide **43** yielded no reaction. Additionally, we attempted deprotection of **42** and **43** using triphenylphosphine and trichlorosilane in THF/toluene (1:1) solution. Interestingly, we detected **46** in both samples, indicating decomposition had again occurred.

Scheme 21

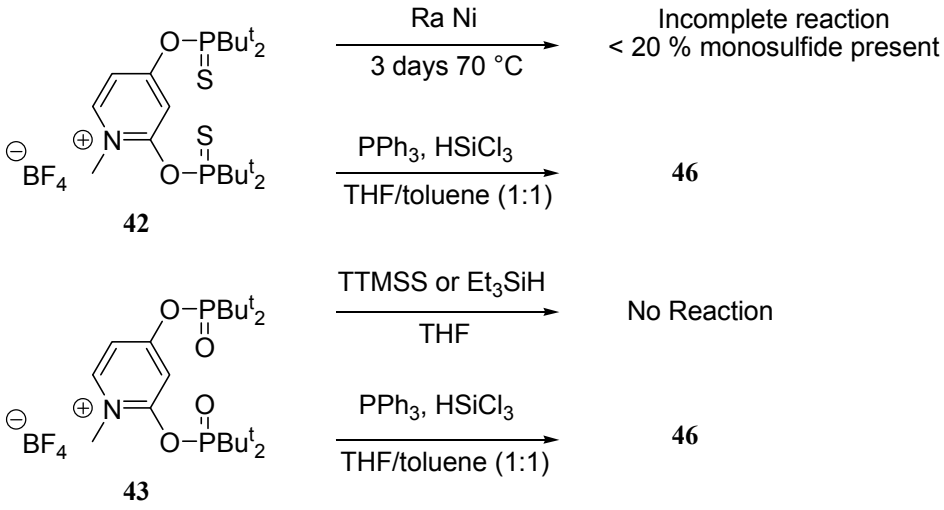

Clearly, the phosphinite linkage in POCOP was susceptible to decomposition. Consequently, **41** – **43** could not be deprotected. Therefore, we decided to abandon protection/deprotection as a strategy for synthesizing POCOP complexes.

3.2 Preparation of Modified POCOP Ligand

We were unable to prepare POCOP complexes with ruthenium and iridium using the proposed ligand **34** due to the availability of nitrogen and formation of a stable five coordinate intermediate **36** (Chart 16).

Chart 16

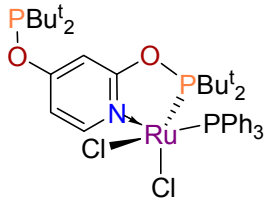

36

This coordination mode was competing with less favorable C-H activation and cyclometalation giving the desired tridentate product. Clearly the availability of nitrogen for metal chelation was a problem. Our options were limited and it was decided that the ligand needed to be modified in order to achieve the desired coordination.

One option that we considered was introducing a methyl group at 6-position on pyridine (Chart 17). This modification would offer some steric protection making nitrogen less available for metal coordination. Should any nitrogen bidentate product

Chart 17

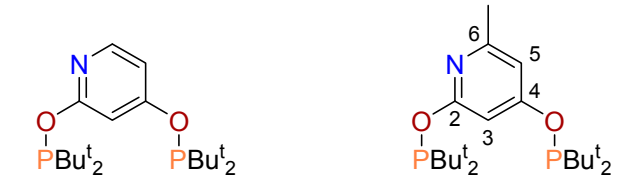

original ligand design — **34**

modified ligand design — **47**

form, the steric repulsion between the methyl group and the metal-ligand environment should be destabilizing (Scheme 22). Continuous heating was expected to result in the formation of a tridentate product.

Scheme 22

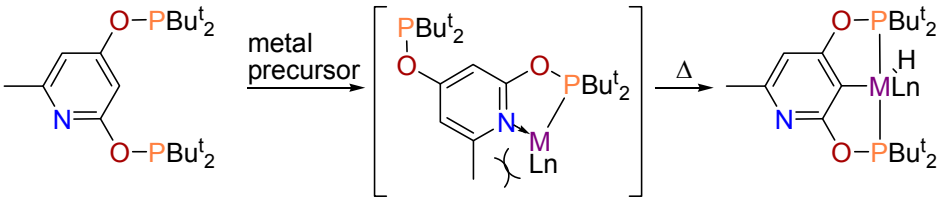

47 — destabilized intermediate

Synthesis of **47** was straightforward as 6-methylpyridine-2,4-diol was commercially available. Phosphinite **47** was synthesized following the same preparation for ligand **34** where the diol was reacted with 2.3 equivalents of di-(*tert*-butyl)chlorophosphine, 3 equivalents of triethylamine in propionitrile and refluxed over a period of 21 h (Scheme 23). Triethylammonium chloride was one of the by-products of this reaction and when the mixture was cooled to room temperature, it crystallized as white needles and was removed through filtration. Propionitrile and excess triethylamine

was removed under vacuum yielding the crude product. It was later determined that the product still contained some triethylammonium chloride. The salt had partial solubility in propionitrile, therefore the product was further purified by extraction in diethyl ether. After removal of the solvent and drying, the product was obtained as an off-white solid.

Scheme 23

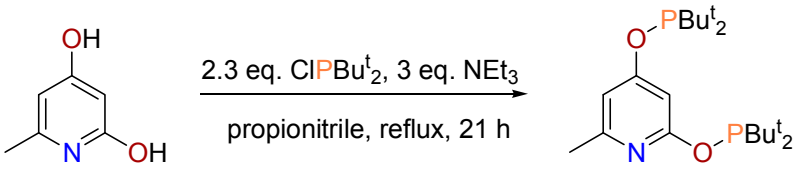

19 **47** 91%

This preparation scaled up well: early synthesis was carried out on a 1.5 g scale and later production increased to approximately 6 g scale. Excellent yields were achieved ranging from 85 to 91%. The product was fully characterized by ^{1}H, ^{13}C, ^{31}P NMR spectroscopy. As expected, we observed two distinct sharp resonances at 153.8 and 153.0 ppm in ^{31}P NMR belonging to the inequivalent phosphorus groups. Once we obtained the modified phosphinite ligand **47**, the next step was metalation.

3.3 Iridium POCOP Complexes

3.3.1 Preparation of Di-μ-chloro-bis[bis(cyclooctene)iridium]

Before beginning investigations with iridium-POCOP coordination, the desired iridium precursor $[IrCl(COE)_2]_2$ was prepared. One advantage when working with di-μ-chloro-bis[bis(cyclooctene)iridium] is that it contains cyclooctene ligands which are labile and easily displaced by stronger coordinating ligands such as phosphines.

The precursor was commercially available, however it was costly and since we are working on a several gram scale, it was more convenient preparing the material in the lab. A preparation for $[IrCl(COE)_2]_2$ was previously described in the literature,[27] however

it gave moderate yields and was carried out on a small scale. Alternatively we were able to modify this synthesis to allow for large scale production of the dimer giving better yields.

Synthesis of $[IrCl(COE)_2]_2$ dimer was achieved via reduction of $IrCl_3 \cdot 3H_2O$ in a 3:1 mixture of water/isopropanol, and cyclooctene followed by 24 hour reflux. An orange oil residue deposited on the bottom of the flask. Upon treatment of the oily material with ethanol the product crystallized and was isolated through filtration. This procedure was practical and allowed for the production of $[IrCl(COE)_2]_2$ on approximately 8 g scale with a reasonable 69 % yield. The iridium dimer was obtained as a yellow/orange solid. The overall balanced equation is illustrated in Scheme 24.

Scheme 24

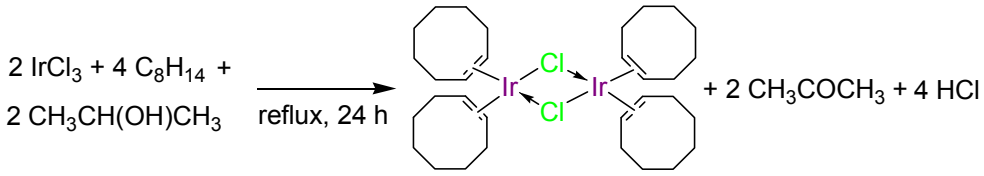

3.3.2 Iridium(POCOP) Hydridochloride Complex

Next the dimer was used in a metalation reaction with POCOP **47**. Synthesis and isolation of the iridium hydridochloride **48** was straightforward. Phosphinite **47** and the iridium dimer were combined in toluene and heated at 110 °C over a period of 24 h. Once toluene was evaporated, the remaining solid material was washed with toluene and hexane yielding the hydridochloride as an orange/red solid (Scheme 25). Trace decomposition of the phosphinite linkage in POCOP pre-ligand was observed, generating approximately 3 % of $HP(O)Bu^t_2$. This was confirmed by ^{31}P NMR as a peak was observed in the phosphine oxide range (~60 ppm) and once proton decoupling was removed, the peak split into two multiplets containing large coupling constant (indicative

of H-P bond). A 15 % excess of POCOP ligand was used to account for the decomposition and to ensure that all of the metal precursor $[IrCl(COE)_2]_2$, was consumed. Overall this synthesis worked well and yields were obtained ranging from 80 to 87 %.

Scheme 25

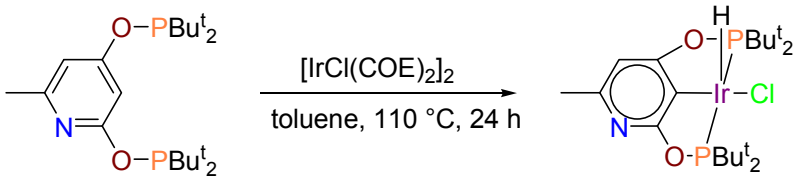

47 **48** 87 %

Ir(III) 16 e$^-$

Mechanistically, the iridium hydridochloride species is generated via a cyclometalation and C-H bond activation reaction of POCOP pre-ligand and iridium precursor. Initially, the iridium dimer dissociates and a phosphinite donor group from POCOP displaces one of the cyclooctene ligands. This is followed by another substitution whereby the second phosphinite group from POCOP displaces another cyclooctene ligand, resulting in a 14-electron trigonal planar iridium(I) intermediate. Finally, the metal center activates the C-H bond at pyridine-C3 immediately followed by oxidative addition giving the 16-electron iridium(III) hydridochloride (Scheme 26).

Scheme 26

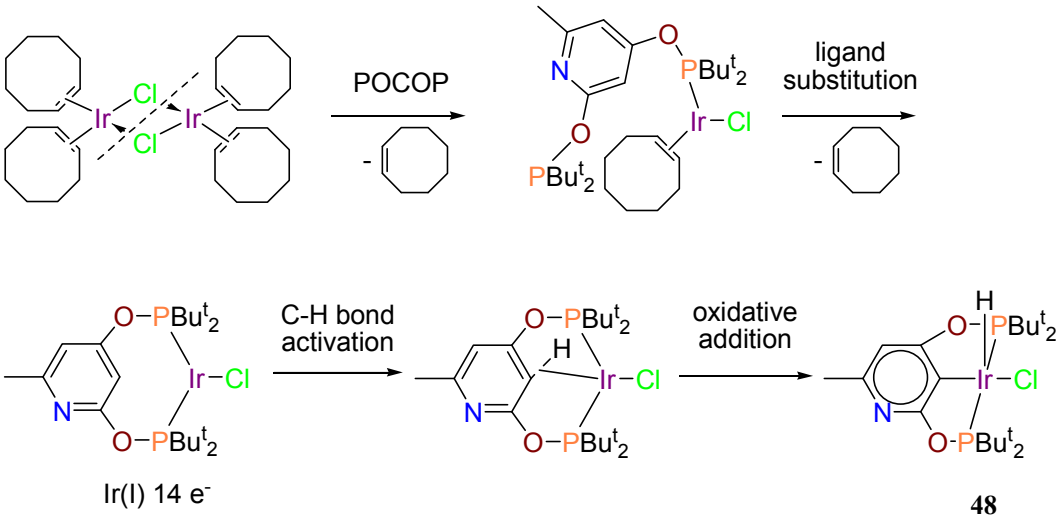

Complex **48** adopts a five coordinate square pyramidal geometry which was confirmed by NMR. Beginning with ^{31}P NMR, we observed that the two distinct peaks once belonging to **47** became two doublets and shifted downfield to 162.5 and 183.5 ppm. The coupling constant indicated that the phosphorus atoms were coupled to each other. Also, large ^{2}J(P-P) of approximately 357 Hz was observed which indicated that the phosphorus atoms were *trans* to one another. Next, ^{1}H NMR was useful in determining the arrangement of the hydride ligand. The hydride appeared as a triplet with a chemical shift of -40.6 ppm, characteristic of hydride ligand *trans* to an empty coordination site. This placed the hydride ligand perpendicular to the coordination plane containing POCOP. Furthermore, a small ^{2}J(P-H) of 13 Hz provided evidence for a *cis* arrangement between the hydride and phosphinite groups. As a result, the chloride ligand was left occupying the remaining coordination site located *trans* to the pyridine-C3 carbon of the POCOP ligand. The pyridine-C3 carbon atom bonded directly to iridium appeared as a multiplet at 107.8 ppm in ^{13}C NMR.

A computational structure for the hydridochloride was optimized by our group and confirms a square pyramidal arrangement (Chart 18). Several interesting bond distances have been shown including a very short Ir-H bond distance of 1.52 Å. Typically, M-H bond distances of row three transition metals fall in the range of 1.65 to 1.75 Å.[28] Another interesting feature is that the phosphorus donor groups are pulled back away from the metal center. The P-Ir-P bond angle gives a good indication of the steric congestion at the site *trans* to Ir-C. In this hydridochloride complex, the P-Ir-P bond angle was 159.8°. This bond angle is influenced by the C-O and O-P bond distances. In this complex, the C-O bond distances were approximately 1.38 Å and the O-P bond distances were 1.68 Å.

Chart 18

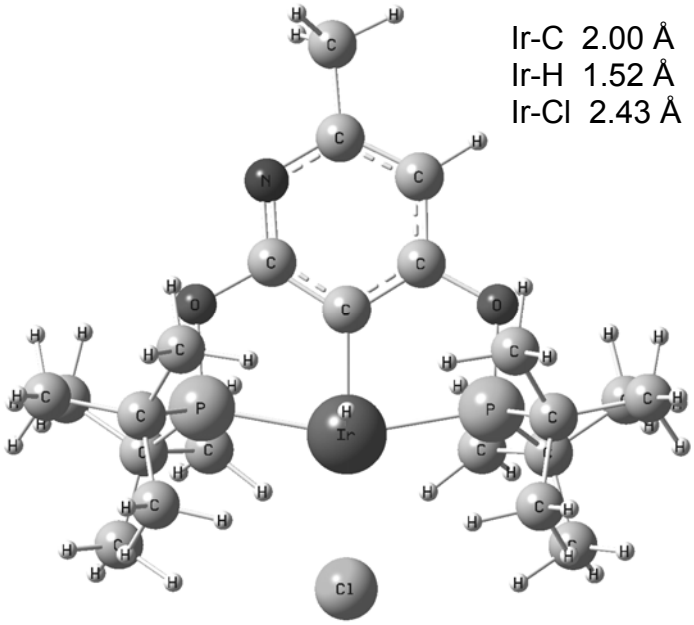

It is noteworthy that the central pyridine-C3 carbon of **48** is not a carbene. The POCOP ligand in **48** is a 5-electron donor. Our next objective was obtaining the iridium-pyridylidene complex which could be attained by alkylating the pyridine nitrogen.

3.3.3 Iridium(POCOP-NMe) Hydridochloride Complex

The next step involved alkylation of the hydridochloride compound **48**. Trimethyloxonium tetrafluoroborate was combined with **48** in dichloromethane and placed in an ultrasonic bath for 2 h (Scheme 27). Dichloromethane was used as solvent for alkylation and as a result high temperatures could not be utilized to drive the reaction. The oxonium salt had limited solubility in dichloromethane, so it was decided that the reaction would take place in an ultrasonic bath which broke down the alkylating agent into fine particulate solid. Initially, vigorous stirring was employed for alkylation; however when the reaction was attempted in the ultra sonic bath, faster reaction times were observed. Isolation of the alkylated iridium hydridochloride complex involved evaporation of dichloromethane followed by washing the resulting solid material with toluene and drying under vacuum. It was important that the alkylating agent was not used in excess as we could not separate it from our product. Alternatively, **48** was well soluble in toluene and excess could be washed away during the workup. Overall, the alkylation worked very well and we achieved yields above 90%.

Scheme 27

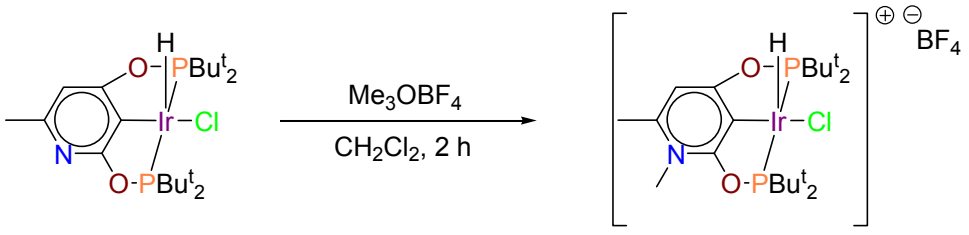

48 **49** 93 %

Ir(III) 16 e$^-$

The 16-electron complex **49** contained a five coordinate square pyramidal geometry. NMR was used to characterize the structure and composition of the compound.

A new ^{1}H NMR signal at 4.0 ppm was observed which corresponded to the methyl group at nitrogen. Furthermore, a triplet belonging to the hydride was observed at -40.0 ppm. The hydride chemical shift was relatively unchanged and as a result its structural assignment remained *trans* to the empty coordination site. The ^{2}J(P-H) was approximately 13 Hz which indicated the hydride was located *cis* to the phosphinite groups. In ^{31}P NMR, the phosphinite doublets shifted farther downfield to 193.7 and 193.4 ppm. Interestingly, the distance between the chemicals shifts narrowed significantly from 19 ppm to approximately 0.3 ppm, after alkylation. The ^{2}J(P-P) remained large at 352 Hz which indicated *trans* orientation of the phosphinite groups. Comparatively, the pyridine-C3 carbon atom bonded to iridium in **49** appeared more downfield in ^{13}C NMR than the previous complex at approximately 114 ppm.

At that point, we obtained a cationic iridium(III) complex. Consequently, we anticipated that the hydride had become more acidic.

A structure for complex **49** was calculated by our group (Chart 19). Clearly the complex adopts square pyramidal geometry with the hydride ligand located perpendicular to the coordination plane containing POCOP-NMe. The Ir-C bond distance remained relatively unchanged at 2.00 Å, while a slightly elongated Ir-H bond distance of 1.53 Å was observed. Slightly shorter Ir-Cl bond distance of 2.40 Å was evident in the alkylated complex. Interestingly, a larger P-Ir-P bond angle of 162.01° was observed in the pyridylidene compound. Also, complex **49** contained shorter C-O bond distances of 1.34 Å and longer O-P bond distances of 1.74 and 1.72 Å.

Chart 19

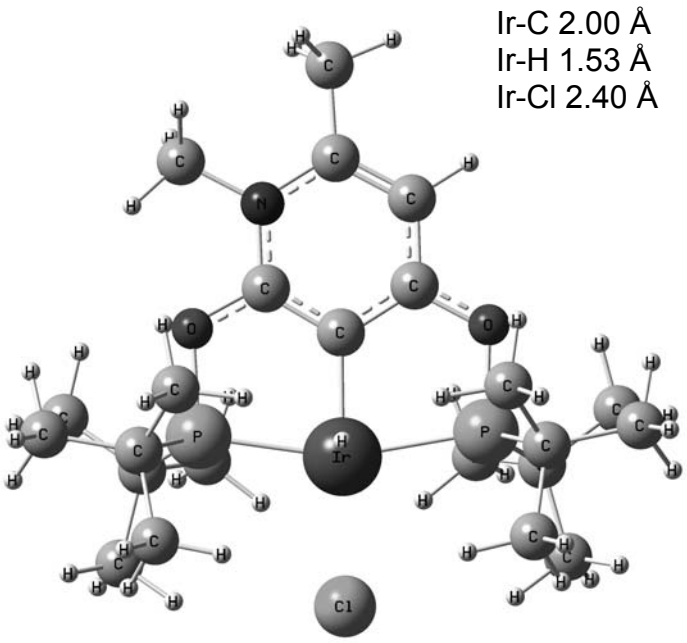

Although a charged carbene compound was obtained, we were more interested in the neutral form of the pyridylidene complex. Thus, the next step in obtaining the neutral complex was a deprotonation reaction of compound **49**.

3.3.4 Iridium(POCOP-NMe) Chloride Complex

The chloride complex **50** was prepared by deprotonation of **49** using 3 equivalents of triethylamine (Scheme 28). THF was selected as the solvent for this reaction instead of dichloromethane, as it was less likely to react with the product chloride compound. Upon addition of base to **49** there was an immediate color change from yellow to a dark red solution. The reaction mixture was left stirring at room temperature for 2 h.

Scheme 28

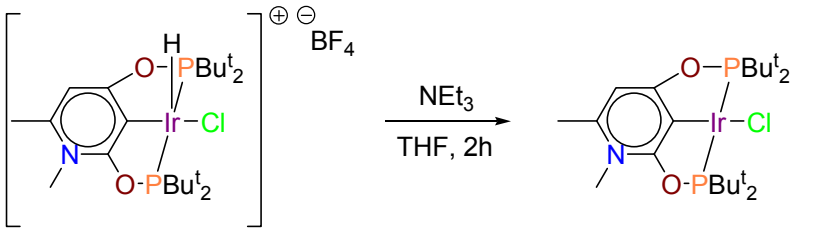

49 **50** 44 %

Ir(I) 16 e$^-$

According to the reaction equation, the only products that are produced during deprotonation are the chloride complex and triethylammonium tetrafluoroborate salt. However, isolation of the chloride complex was not trivial, as we attempted several strategies including product extraction, washing, and crystallization. We observed a phosphorus containing impurity in the *tert*-butyl range of ^{1}H NMR. This impurity could have resulted from formation of a solvent complex between the chloride complex and THF. The product chloride produced from deprotonation was coordinatively unsaturated and contained two available coordination sites, thus it was capable of incorporating a THF molecule into one of the unoccupied sites (Chart 20). A combination of extraction followed by crystallization from toluene generated the most pure product although we obtained poor yields (~40%). Most of the material was lost due to incomplete crystallization of the chloride complex. The product was obtained as a dark orange solid.

Chart 20

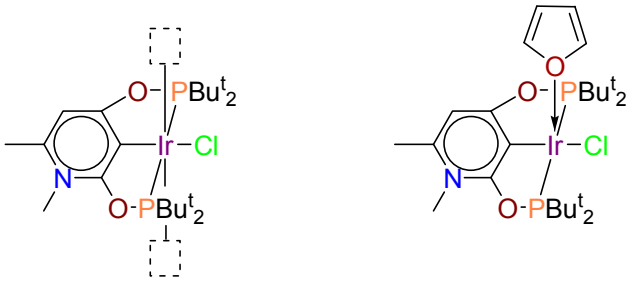

2 available coordination sites THF-complex

Deprotonation of complex **49** yielded a 16-electron iridium(I) (POCOP-NMe) compound **50**. The product compound was four-coordinate and adopted a square-planar molecular geometry. NMR was used to characterize the structure and composition of the chloride. Beginning with ^{1}H NMR, we immediately noticed the disappearance of the hydride resonance. Also, we confirmed that no reactions occurred at pyridine-H, CH_3 and NCH_3. Trace amounts of toluene and THF solvent impurities were detected. In ^{31}P NMR, the chemical shifts of the phosphorus groups were located at 191.7 and 191.6 ppm. The distance between the chemical shifts continued to narrow. A *trans* arrangement of the phosphinite groups was confirmed due to a large ^{2}J(P-P) of 417 Hz. Attempts to produce good quality crystals for structural analysis were unsuccessful.

3.3.5 Reactions of Iridium(POCOP-NMe) Chloride Complex

Initially, we attempted a hydrogen addition to the [IrCl(POCOP-NMe)] complex. Crabtree reported oxidative addition of hydrogen to various square planar iridium(I) complexes containing phosphine ligands (Chart 21).[29] Iridium hydrido complexes they studied were prepared under H_2.

Chart 21

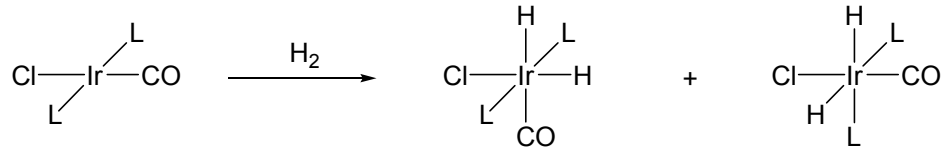

Similarly we prepared a sample of the chloride **50** under H_2 anticipating that an 18-electron dihydrido would be produced (Scheme 29). Unfortunately this was not the case and we observed no reaction under hydrogen.

Scheme 29

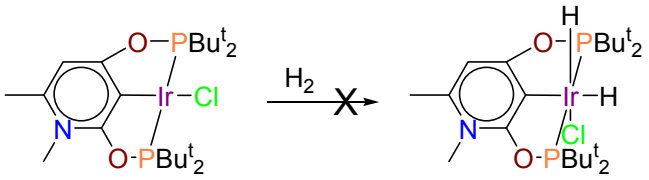

50

Ir(III) 18 e$^-$ dihydrido chloride complex

The product dihydride complex does not form as it is possibly less stable than chloride **50** due to the strong *trans* effect and *trans* influence of the hydride ligands. In the dihydrido complex, there is a hydride located *trans* to the carbene of pyridine which is a very unfavorable arrangement.

Our next challenge lied in the preparation of the hydride species **51** from the chloride complex **50**. Transition metal hydrides are commonly prepared via metathesis reaction involving a metal halide and a main group hydride donor. This generates a halide salt along with the corresponding transition metal hydride. We studied two reagents as possible hydride donors: lithium triethylborohydride (Li[HBEt$_3$]) and potassium hydride (KH).

Lithium triethylborohydride is commonly used reagent for the preparation of transition metal hydrides as it poses no risk of forming borohydride or aluminohydride complexes of the type $L_nM(\eta^3\text{-}QH_4)$ (Q = B or Al), which may occur when other borohydride reagents, such as sodium borohydride ($NaBH_4$), are used.[30]

Preparation of **51** using lithium triethylborohydride as hydride source was attempted first. A sample was prepared in THF containing 2 equivalents of Li(HBEt$_3$) and [IrCl(POCOP-NMe)] under H_2 (Scheme 30). No reaction was observed at room temperature or at 50 °C.

Scheme 30

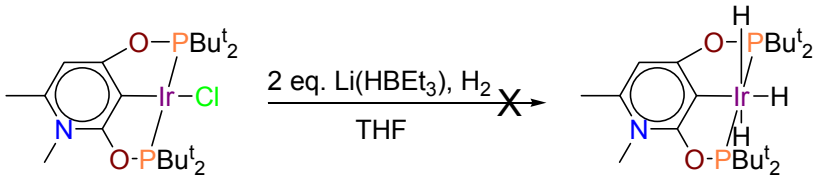

50 **51**

Ir(I) 16 e$^-$ hydrido complex

We assumed the lack of reactivity of the chloride **50** towards Li(HBEt$_3$) was due to the bulky size of the hydride source. Consequently, we prepared a different sample in THF utilizing the less bulky potassium hydride (Scheme 31). There was no immediate reaction visible which was later confirmed by NMR. Potassium hydride was too insoluble in THF for any reaction to occur. Thus, it was necessary to use a phase transfer catalyst 18-crown-6 to dissolve KH in THF and facilitate the reaction. Once KH dissolved in solution there was still no evidence that a reaction had occurred.

Scheme 31

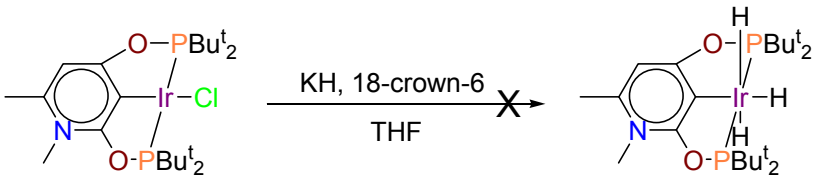

50 **51**

Ir(I) 16 e$^-$ hydrido complex

Our next step towards the synthesis of **51** involved treatment of the chloride **50** with potassium *tert*-butoxide (KOBu^t) in 2-propanol. Chloride abstraction generates a cationic iridium complex. This is followed by removal of the hydroxy hydrogen atom from 2-propanol by the butoxide anion, yielding *tert*-butanol and 2-propoxide anion. Lastly, 2-propoxide coordinates to the cationic iridium complex which is followed by β-hydride elimination generating the iridium hydrido complex and propanone.

An NMR tube reaction was prepared containing the **50** and 1 equivalent of potassium *tert*-butoxide in 2-propanol (Scheme 32). Unfortunately, we observed no reaction at room temperature or heating at 50 °C.

Scheme 32

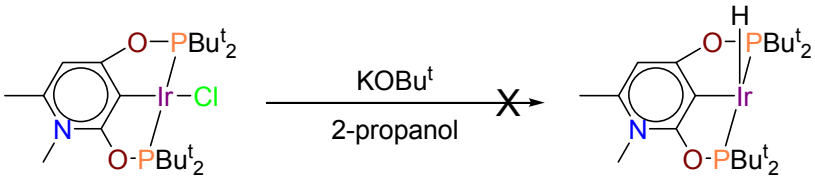

50 **51**

Ir(I) 16 e$^-$ hydrido complex

Since synthesis of the iridium(POCOP-NMe) hydrido complex was unsuccessful, our next challenge lied in exploring the catalytic activity of the iridium(POCOP-NMe) chloride complex.

Milstein[31] and Jensen[32] presented examples of phosphino-palladium PCP **51** and POCOP **52** pincer complexes used in homogeneous catalysis of carbon-carbon coupling reactions, namely the Heck reaction (Chart 21). Comparatively, our iridium(POCOP-NMe) chloride complex is isoelectronic with complexes **52** and **53**. As a result, we screened the catalytic activity of complex **50** in Heck-type reaction.

Chart 22

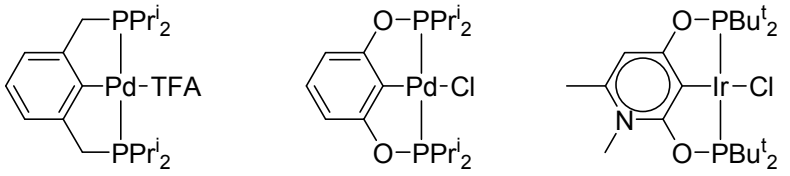

Pd(II) 16 e$^-$ d^8 Pd(II) 16 e$^-$ d^8 Ir(I) 16 e$^-$ d^8

52 **53** **50**

A sample containing 1.5 equivalents of bromobenzene, and 1 equivalent of methyl acrylate (MA), and 0.25 mol% of chloride **49** (with respect to MA) was prepared and

heated at 85 °C for 4 h (Scheme 33). The reaction mixture quickly became more viscous to the point of solidification. The increase in viscosity was a good indication that oligomerization had occurred. A single new resonance corresponding to carbonyl carbon was observed in ^{13}C NMR. Based on this information, we concluded that selective formation of oligomerized MA product had occured (n = narrow range of integers).

Scheme 33

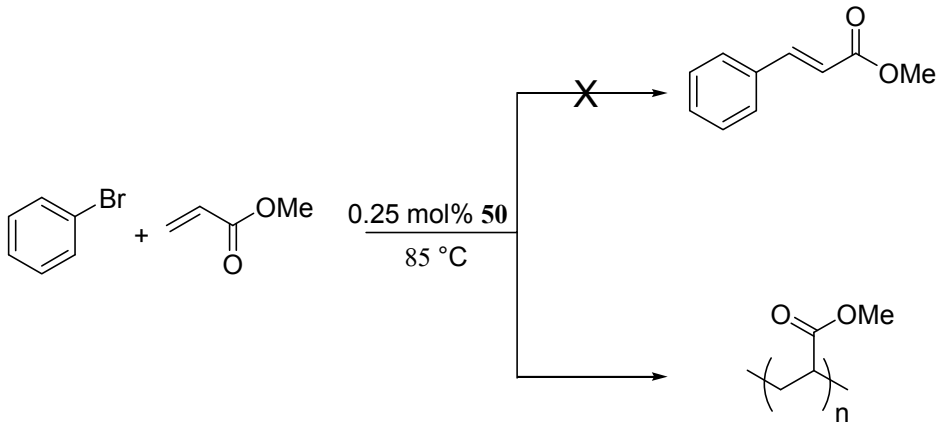

In light of this development, further investigation into whether the catalyst was responsible for clean selective production of oligomerized MA was needed. Accordingly, a new sample containing MA, C_6D_6 and complex **50** was prepared (Scheme 34). The sample was heated at 85 °C for a period of 24 h to ensure the reaction had gone to completion. Once more, the new sample had solidified; however, this time multiple peaks belonging to carbonyl carbons were observed which was an indication that various oligomer products had formed (n = wide range of integers). As a result, no further investigations were carried out.

Scheme 34

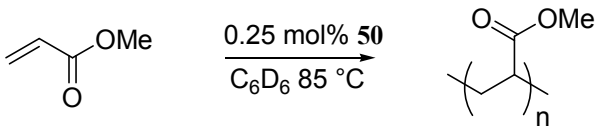

3.4 Ruthenium POCOP Complexes

3.4.1 Preparation of Di-μ-chloro-bis[chloro(p-cymene)ruthenium]

We screened two metalation precursors, di-μ-chloro-bis[chloro(*p*-cymene)ruthenium] and tris(triphenylphosphine)ruthenium(II) dichloride, in NMR tube reactions. After extensive heating over a period of days, we could not detect evidence of the desired metalation product in the sample containing $RuCl_2(PPh_3)_3$. Conversely, we observed formation of a major cyclometallated product after heating over 24 h in the sample containing $[RuCl_2(p\text{-cymene})]_2$. Thus, $[RuCl_2(p\text{-cymene})]_2$ was selected as the precursor for the ruthenium(POCOP) chemistry.

The precursor was prepared on a 5.87 g scale by reaction of ruthenium trichloride, and R-α-phellandrene in 2-propanol. After heating the mixture at 95 °C for 5 h, 1 equivalent of 2,6-lutidine was added heated at 95 °C for 15 h. The ruthenium *para*-cymene compound was isolated by crystallization at low temperature (-15 °C) from 2-propanol followed by filtration, washing with ethanol and drying. Overall, the synthesis worked very well to give the product in 88% yield as a dark brown solid (Scheme 35).

Scheme 35

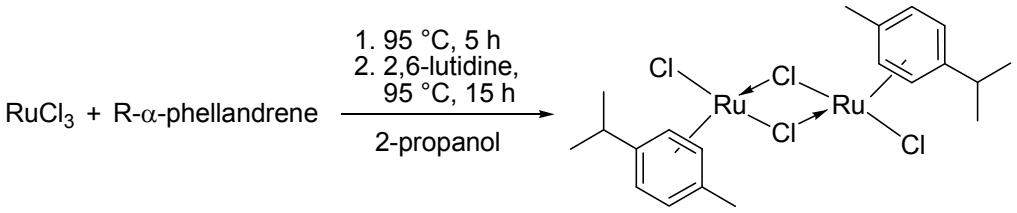

3.4.2 Ruthenium(POCOP-NH) Hydridochloride

Our next objective was to prepare a ruthenium (POCOP) complex from the ruthenium dimer and **47**. A preliminary NMR tube reaction containing 1.5 equivalents of **47**, and 0.5 equivalents of ruthenium dimer in 2-propanol was heated at 90 °C for 24 h.

Afterwards, in ^{31}P NMR we observed that there was starting material remaining. Also, there were two main compounds formed in a 2:3 ratio, a minor product consisting of a ruthenium(POCOP) complex, and a major product which was identified as HP(O)(Bu^t_2). Pincer complexes of the POCOP type are known for being robust and thermally stable thus product decomposition was likely not occurring. However, once proton decoupling was removed from ^{31}P NMR the chemical shift split into two multiplets with a large coupling constant, consistent with H-P coupling. Clearly, we had observed decomposition of the phosphinite linkage in POCOP reactant.

A series of NMR tube reactions were prepared in an attempt to optimize the product conversion. Firstly, we decided to use 20% less of the POCOP pre-ligand to minimize the amount of HP(O)(Bu^t_2) produced. Furthermore, since HCl was a product of this reaction, we decided to use 3 equivalents of 2,6-lutidine as base. The reaction was optimized varying parameters including temperature, and solvent (Table 2).

Table 2

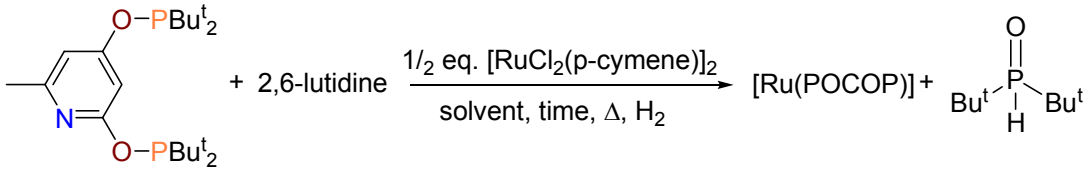

1.2 eq. **47** 3 eq. **54** **46**

Entry	Solvent	Temperature	Time	Conversion	
	(0.035 mM)	(°C)	(h)	**54** (%)	**46** (%)
1	2-propanol	90	24	68	27
2	2-pentanol	90	3	0	40
3	2-pentanol	110	3	0	30

We observed significant ligand decomposition in 2-pentanol at 90 and 110 °C after very short 3 h (Entry 2 and 3). Reaction in 2-propanol with 2,6-lutidine gave the

highest conversion of ruthenium(POCOP) complex with smallest amount of di(*tert*-butyl)phosphine oxide (Entry 1).

After the metalation reaction was optimized, we attempted synthesis of the ruthenium(POCOP) complex on a larger 1 g scale. The ruthenium complex was synthesized via reaction of 1.2 equivalents of POCOP pre-ligand, ½ equivalent of $[RuCl_2(p\text{-cymene})]_2$, and 3 equivalents of 2,6-lutidine under H_2 in 2-propanol (Scheme 36). The mixture was heated to 85 °C for 20 h which gave a dark red solution containing the desired product compound.

Scheme 36

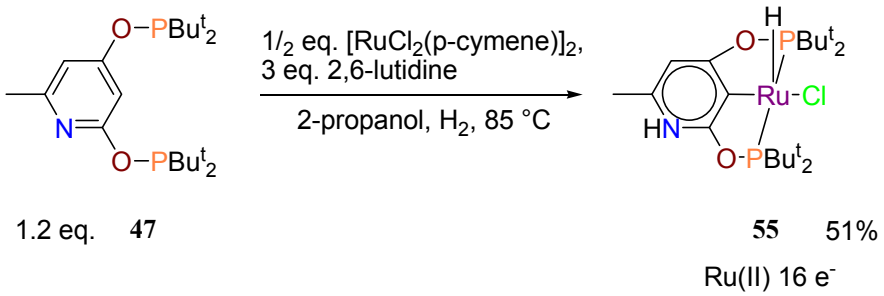

1.2 eq. **47** **55** 51%

Ru(II) 16 e$^-$

Isolation of the product compound was not trivial as the reaction mixture contained 2,6-lutidinium hydrochloride, di(*tert*-butyl)phosphine oxide and **55**. Typically pincer-type phosphine complexes have limited solubility in alcohols, thus we initially attempted to isolate the product by crystallization from 2-propanol at low temperatures (-15 °C). This was unsuccessful and nothing precipitated from solution. Next, 2-propanol was removed under vacuum which yielded a dark sticky red solid. Our next isolation strategy involved product extraction from the crude material using a hydrocarbon solvent such as toluene. During extraction we observed that the product compound had limited solubility in toluene and could not be completely extracted. In light of this result, we decided to wash the crude material with water to remove the lutidinium salt, followed by

dissolving the remaining material in a large quantity of toluene. The toluene solution was concentrated to approximately one quarter its original volume. At this point the product material was crystallized from the solution at low temperature (-15 °C). After decantation and washing, pure product was obtained as a red solid in 51% yield.

Complex **55** was structurally characterized by NMR. Interestingly, we observed formation of a 16-electron square pyramidal pyridylidene complex **55** and not the anticipated dihydrido chloride species **56** (Chart 23). Beginning with ^{1}H NMR, a triplet was observed at -30.4 ppm which corresponded to a hydride coupled to two phosphorus atoms. Highly upfield chemical shifts, as observed, are consistent with a hydride ligand *trans* to an empty coordination site. Comparatively, protonated nitrogen appeared as a single broad peak downfield at 12.4 ppm.

Chart 23

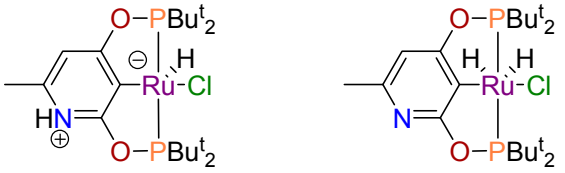

55
pyridylidene form

56
dihydride form

Optimized structures of **55** and **56** were calculated by our group and illustrated in Chart 24. Calculated bond distances allow for structural comparison of the pyridylidene and dihydride forms. Interestingly, a shorter Ru-C bond length of 1.98 Å was observed in the pyridylidene form **55**, compared to the bond length of 2.02 Å observed in form **56**. Greater *trans* influence on the chloride ligand was observed in the pyridylidene form, as the complex contained a elongated Ru-Cl bond of 2.45 Å when compared to the bond distance of 2.40 Å in the dihydride form.

Chart 24

Atomic distances (Å)

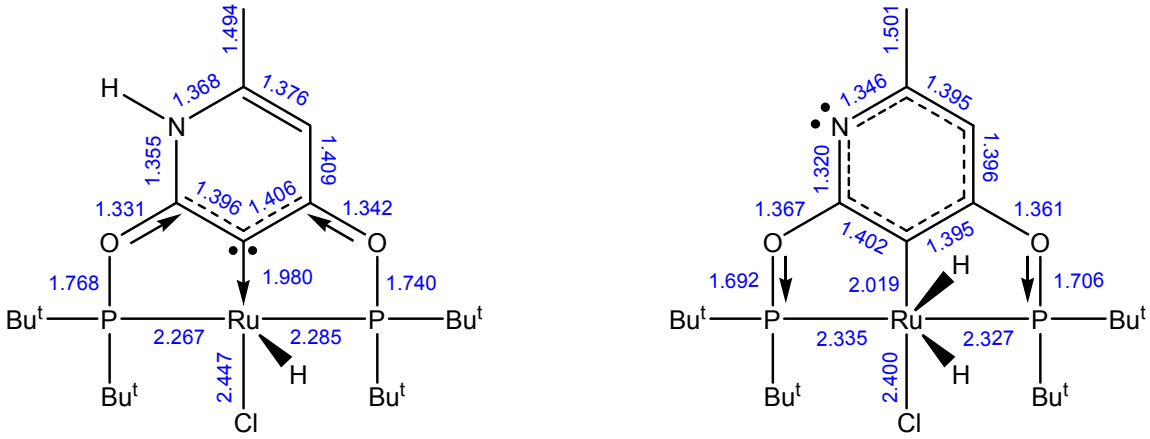

In addition, the atomic polar tensors (APT) charges were calculated and give good estimates of the atomic charges in both structures (Chart 25). A significantly more negative charge was present on ruthenium in **55** than **56**, due to the strong electron donor character of the PyC3 system.

Chart 25

APT atomic charges (e^-)

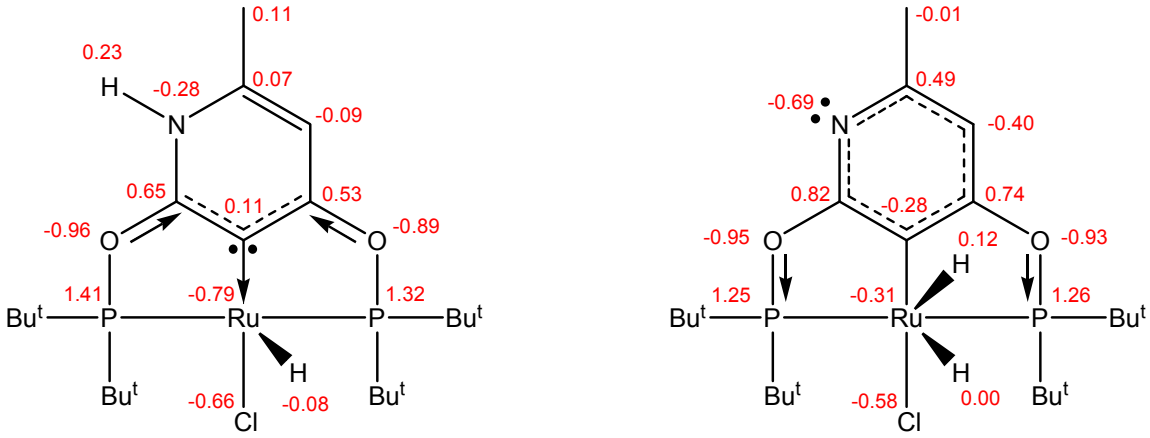

3.4.3 Ruthenium Dihydrogen Complexes

Hydridochloride **55** served as an entry point into the ruthenium chemistry studied. Preliminary NMR tube reactions indicated that a dihydrogen complex could be prepared from **55**.

Characterization of dihydrogen complexes can be quite challenging. Due to the short H-H distance of H_2 ligands, they exhibit rapid relaxation times. Additionally, there is exchange of hydrogen within the system, thus chemical shifts of H_2 and neighboring hydride ligands are typically averaged and appear as a single resonance. However, low temperature NMR can be utilized to slow hydrogen exchange resulting in de-coalescence of the averaged signal. Furthermore, deuterium can be introduced into the system giving rise to H-D complexes. The *J*(H-D) can be measured which gives useful information regarding H-H bond distances.

Kubas et al. discovered the first dihydrogen complexes *mer-trans*-$M(CO)_3(PCy_2)_2(H_2)$ (M = Mo, W) in 1984. These complexes were obtained by addition of H_2 to unsaturated complexes $M(CO)_3(PCy_2)_2$ (M = Mo, W).[33] Similarly, we wished to generate a dihydrogen species from the 16-electron **55** by either addition of H_2 ligand **57** or by displacement of HCl **58** (Scheme 37). However, no reaction was observed when complex **55** was exposed to H_2 atmosphere.

Scheme 37

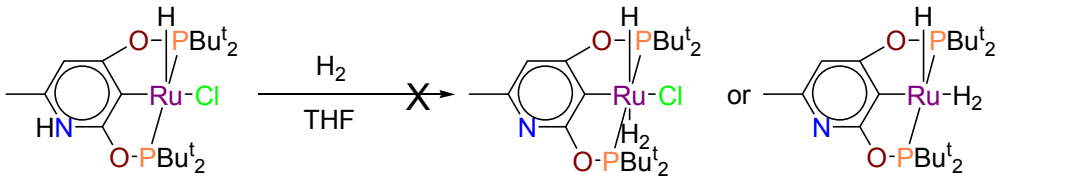

55 **57** product of addition **58** product of displacement

The next step towards synthesis of dihydrogen complex involved treatment of **55** with either $KOBu^t$ or $Li[HAl(OBu^t_3)]$ in the presence of a H_2 source. After dehydrochlorination, the unsaturated compound is available for dihydrogen coordination. Two potential sources of H_2 ligand include alcohols such as 2-propanol (incompatible with metal hydride reagents) and hydrogen gas.

Initially we prepared an NMR tube reaction containing **55**, 1.5 equivalents of $KOBu^t$ in THF-d8 under H_2 (Scheme 38). Potassium tert-butoxide appeared to have reacted completely within several minutes and the solution maintained a red color. ^{31}P NMR indicated that the hydridochloride had completely reacted. Two new doublets belonging to a major compound were detected at 232.2 and 209.7 ppm, which was believed to be the expected dihydrogen complex **58**. Furthermore, a single, broad resonance located at approximately -12 ppm was observed in ^1H NMR which was consistent with a H_2 ligand. In addition to the dihydrogen complex, several minor by-products were detected totaling approximately 25%. As a result, this sample was unsuitable for proper characterization of the dihydrogen compound.

Scheme 38

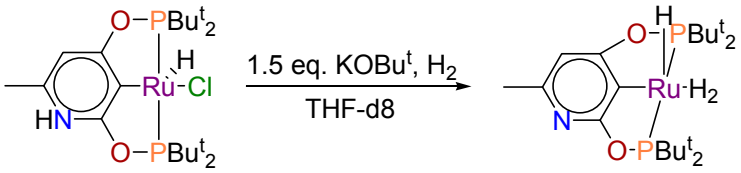

55 **58**

In light of these results, we decided to prepare another sample in THF-d8 containing **55**, 1.1 equivalents of $Li[HAl(OBu^t)_3]$ and under H_2 (Scheme 39). It had appeared as though a reaction had occurred and the solution maintained its red color. In ^{31}P NMR, we observed relatively clean formation of a single compound bearing similar

chemical shift as the suspected dihydrogen complex from the previous reaction. In ^{1}H NMR, a single, broad resonance was observed at approximately -13 ppm. Additional work was necessary in order to fully characterize the new compound.

Scheme 39

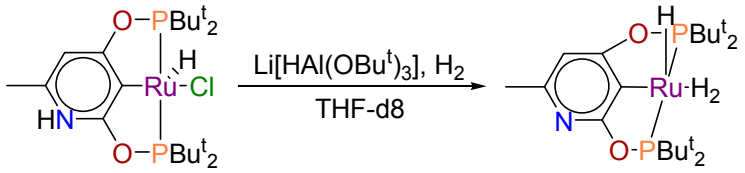

55 **58**

Next we wished to perform low temperature NMR in order to determine structure of the newly generated dihydrogen complex. Interestingly in ^{31}P NMR, the two doublets observed at room temperature which corresponded to the dihydrogen complex had split into four doublets located at 236.6, 233.2, 214.5, and 210.6 ppm at -80 °C. This was an indication that the sample contained two similar compounds undergoing rapid exchange at room temperature. Additionally, another broad resonance was detected at 206.17 ppm. In ^{1}H NMR the broad resonance observed at approximately -13 ppm de-coalesced nicely into several broad single peaks as illustrated by the bottom spectra in Chart 26.

Chart 26. ^{1}H NMR at -80 °C under H_2 and D_2.

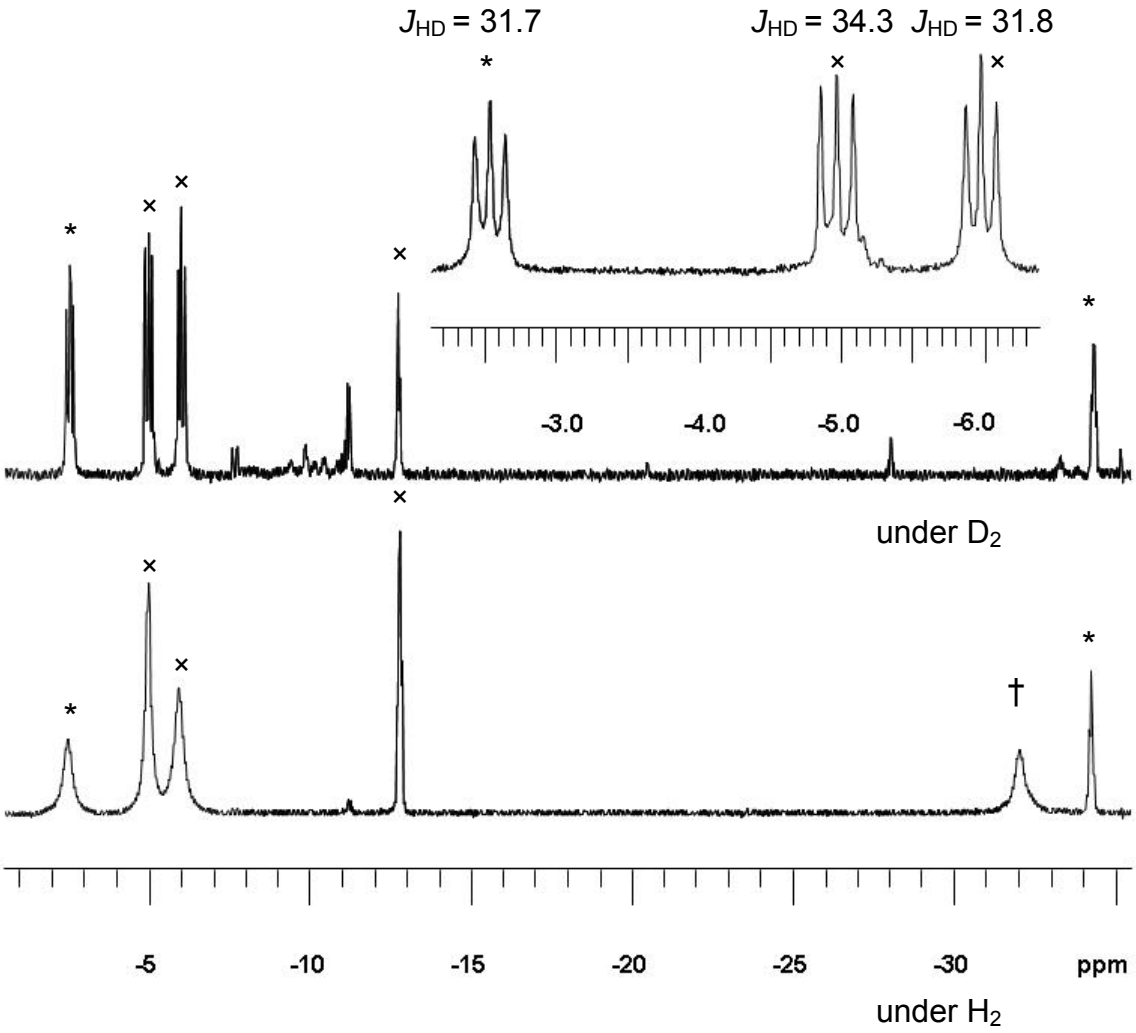

From this spectrum, we determined that there were three different compounds present in the sample: dihydrogen complex **58**, bis-dihydrogen complex **59** and a mono hydrido complex **60** (Chart 27). In Chart 26, the chemical shifts belonging to **58** are denoted by *, **59** by ×, and **60** by †. Beginning with **58**, the chemical shift at -2.5 ppm integrated for two protons and belonged to a single H_2 ligand. One hydrogen was detected further up field at -34.3 ppm characteristic for hydride ligand positioned *trans* to an empty coordination site. In contrast, the hydride ligand in the bis-dihydrogen complex was detected further downfield at -12.7 ppm, indicating an arrangement *trans* to a H_2

ligand. Furthermore, two H_2 ligands bearing chemical shifts -5.0 and -6.0 ppm and belonging to the bis-dihydrogen complex **59**, were identified. Lastly, we believed that a mono hydrido compound **60** was present due to a hydride resonance detected at -33.3 ppm, indicating it was *trans* to an empty coordination site.

Chart 27

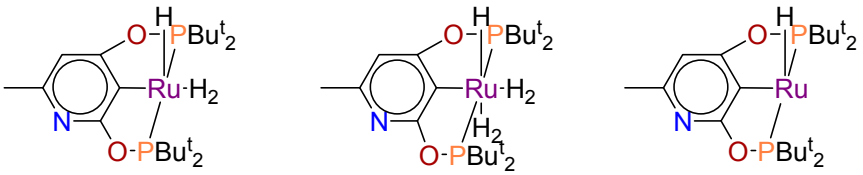

58 **59** **60**

Next we wished to saturate the same sample with D_2 in order to incorporate deuterium into the complexes and measure the resulting *J*(H-D). First we performed several freeze-pump-thaw cycles on the sample. Interestingly, we observed a drastic change in color from red to deep purple, typical of very unsaturated complexes. The sample was refilled under D_2 and the red color returned.

Once the sample was prepared, low temperature NMR was repeated at -80 °C as illustrated as the top spectrum in Chart 25. Luckily, we noticed well resolved triplets in the high field range in ^{1}H NMR, indicating direct H-D bonding in the complexes. The *J*(H-D) were measured to be 31.7 Hz for the dihydrogen complex, 34.3 and 31.8 Hz for the bis-dihydrogen complex. These values are evidence of short H-H bonding. The deuterium content was calculated to be approximately 85 %. Interestingly, the hydride resonance belonging to **60** had disappeared. Also, there were more impurities present likely due to some decomposition.

A computational structure for **58** was optimized by our group and supports the proposed structural geometry derived from the NMR data (Chart 28). It is noteworthy

that the newly generated dihydrogen complexes are no longer pyridylidene complexes. The dihydrogen ligand is coordinated in an η^2 mode and occupies the site cis to the hydride ligand. The calculated H-H distance in the dihydrogen ligand was 0.88 Å, marginally larger than that of free H_2 (0.74 Å).[33] The hydride ligand occupied the site perpendicular to the plane containing POCOP and *trans* to the empty coordination site. The calculated bond lengths of Ru-H and Ru-C were 1.54 Å and 2.04 Å, respectively. Furthermore, a P-Ru-P bond angle of 156.2° was observed.

Chart 28

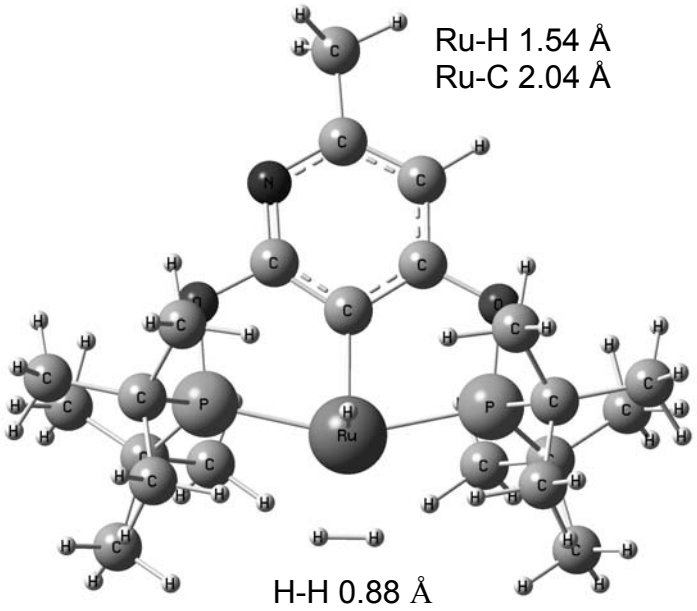

In addition, an optimized structure of **59** was generated and is in agreement with the proposed octahedral geometry derived from NMR data (Chart 29). The new H_2 ligand occupied the coordination site *trans* to the hydride. A slightly shorter H-H distance of 0.84 Å was observed compared to 0.88 Å belonging to the adjacent H_2 ligand. Interestingly, an elongated Ru-H bond of 1.59 Å was observed. The lengthening was possibly due to the *trans* influence from the H_2 ligand opposite to the hydride. Similarly

Ru-C bond lengthening to 2.06 Å was observed in **59**. In contrast, a smaller P-Ru-P bond angle of 154.1° was detected in the bis-dihydrogen complex, a result further accommodation of an additional H_2 ligand.

Chart 29

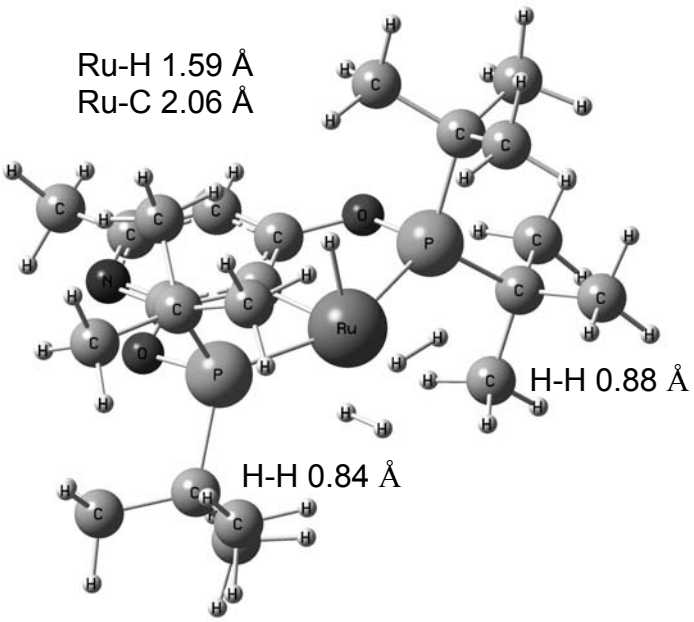

3.4.4 Reactions of Ruthenium(POCOP-NH) Hydridochloride

As demonstrated in the previous section, dehydrochlorinated **55** reversibly coordinates H_2. This motivated us to investigate potential catalysis in ketone hydrogenation reaction. Hydrogenation of acetophenone is a commonly used reaction for the evaluation of prospective hydrogenation catalysts and will be the focus of this section.

We prepared a reaction solution containing acetophenone, 0.1 mol% of **55** and 1.5 equivalents of $KOBu^t$ (Scheme 40). The solution was heated to 100 °C under H_2 for 20 h yielding a dark brown solution. An NMR sample was taken from the solution and confirmed formation of a moderate amount of 1-phenylethanol with a TON of 130.

Ketone hydrogenation did not look promising and as a result no further investigations were carried out.

Scheme 40

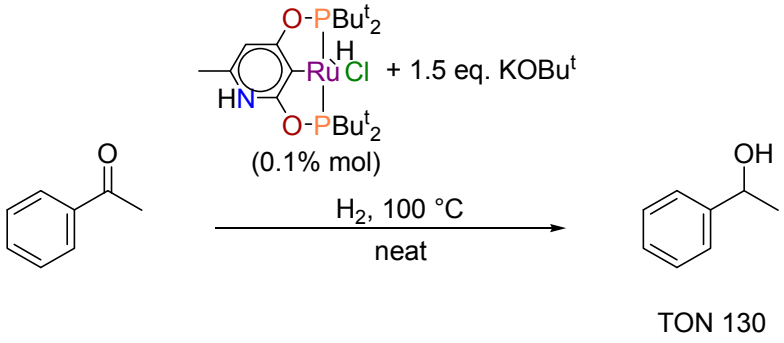

3.4.5 14-Electron Ruthenium(POCOP) Hydride

Although rare and unusual, 14-electron ruthenium compounds have been prepared and documented in the literature.[26] We thought it would be interesting to attempt isolation and characterization of the 14-electron ruthenium species **60**, detected during our studies of the dihydrogen complexes.

The 14-electron complex can be synthesized via dehydrochlorination of **55**. We prepared a reaction mixture containing the hydridochloride **55**, 1 equivalent of KOBu^t in 2-propanol (Scheme 41). Potassium *tert*-butoxide was selected over Li[HAl(OBu^t)$_3$] to avoid difficulties during isolation. Dehydrochlorination by KOBu^t would generate KCl and HOBu^t as by products. The reaction mixture was stirred at room temperature for 1 h followed by evaporation of 2-propanol and dried for 2 h. This generated a deep purple solid which was indicative of presence of an unsaturated compound. After drying, we isolated the product by extraction in toluene followed by evaporation of the solvent under vacuum, yielding a shiny deep purple solid.

Scheme 41

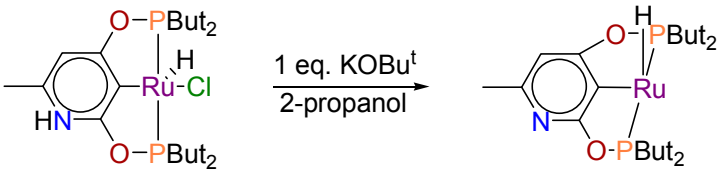

54 **59**

Ru(II) 14 e-

Next, we attempted characterization by preparing an NMR sample in hydrocarbon solvent C_6D_6. Unfortunately, in ^{1}H NMR we observed several broad, unresolved, hydride resonances in the -30 ppm region. Similarly, we observed multiple broad resonances in ^{31}P NMR. The NMR data clearly showed evidence that several products were present, however we were not certain whether the presence of multiple compounds was a result of decomposition. In some instances, formation of solvent complexes or intramolecular agostic interactions have been observed with highly unsaturated complexes and can result in complicated NMR behaviour.

Consequently we prepared samples in solvents capable of coordinating to **60**: acetonitrile and THF. In the sample containing acetonitrile, we observed clean formation of a single compound in ^{31}P NMR, evidence that decomposition had not occurred during the preparation of **60**. Furthermore, in ^{1}H NMR a hydride resonance was detected at -23.2 ppm. The chemical shift was located farther downfield suggesting the hydride was no longer *trans* to an empty coordination site, instead it was *trans* to an acetonitrile ligand. As a result, there must have been a second acetonitrile ligand present *cis* to the hydride. Therefore, we propose that **60** forms a solvent complex **61** with two molecules of acetonitrile (Chart 30). In contrast, the sample prepared in THF showed formation of two compounds. A major compound which we suspected was a THF complex **62** and a minor

compound which was likely **60**. Further investigation was required into the characterization of the THF complex.

Chart 30

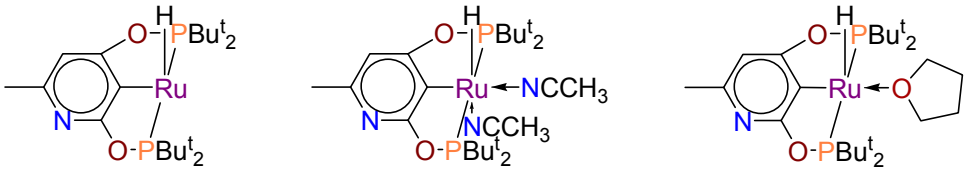

60 **61** **62**

RuH -23.2 ppm

Additional information concerning the structure and geometry of **60** was obtained from an optimized structure calculated by our group (Chart 31). The overall molecular geometry of **60** was see-saw. Interestingly, the hydride remains positioned perpendicular to the plane containing the POCOP ligand. The Ru-H bond distance was 1.54 Å, relatively unchanged from the Ru-H bond length in the hydridochloride complex **55** (1.55 Å). Similarly, the Ru-C bond distance in **60** was 1.97 Å, similar to the bond length observed in **55** (1.98 Å).

Chart 31

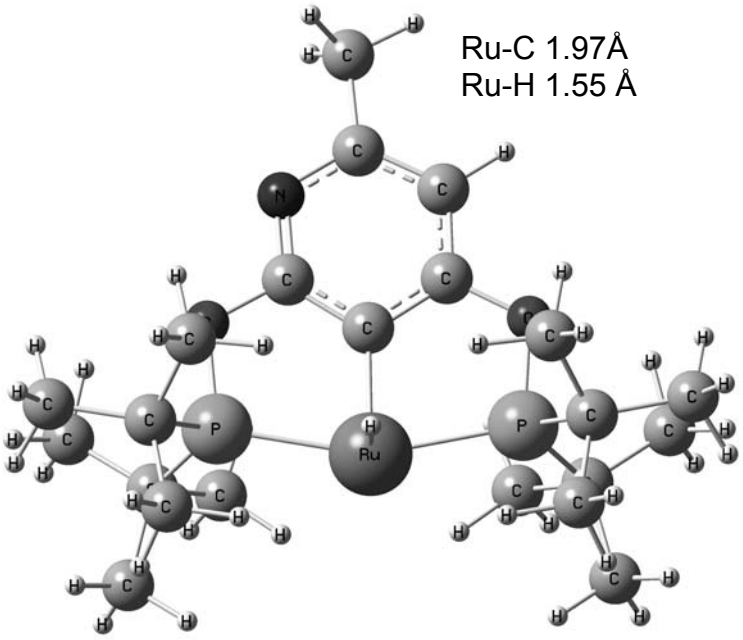

3.4.6 Reactions of 14-Electron Ruthenium(POCOP) Hydride

Following its preparation, we decided to investigate the potential catalytic properties of **60**. As mentioned previously in Section 1.4, Brookhart et al. developed a complex useful for alkane dehydrogenation. Compound **63**, generated in situ, was 14-electron and the active species for this type of catalysis (Chart 32). Comparatively, compound **60** was isoelectronic and structurally related with **63**. We thought it would be interesting to evaluate the catalytic activity of **60** in alkane dehydrogenation.

Chart 32

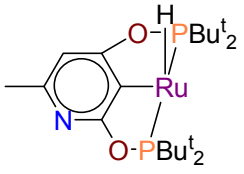

60

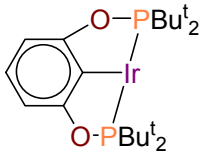

63

Brookhart's active catalyst
for alkane dehydrogenation

Catalytic activity of **60** was screened in the commonly used benchmark reaction, alkane dehydrogenation of cyclooctane (Scheme 42). We prepared a reaction mixture containing a 3.6:1 ratio of cyclooctane to tbe, and 0.1 mol% (with respect to cyclooctane) of **60**. The amount of tbe was kept low in order to minimize catalyst inhibition. The reaction mixture was heated to 135 °C overnight. Bubbling was observed during this time which can possibly be attributed to H_2 evolution. After approximately 20 h the reaction mixture had changed color from purple to brown.

Scheme 42

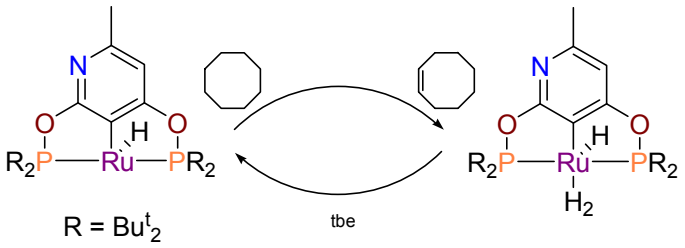

A sample was prepared analyzed by NMR which showed trace amounts of cyclooctene present. It had appeared as though alkane dehydrogenation was taking place, however additional work was needed to obtain quantitative results.

4.0 Conclusion

In conclusion, we synthesized and characterized a new pyridine-based POCOP pincer ligand. Subsequently, ligand metalation gave rise to the first pyridylidene POCOP pincer complexes of ruthenium and iridium. The structural and electronic properties of these complexes were investigated yielding information concerning bond angles and bond distances. Ruthenium(POCOP) dihydrogen complexes were prepared from the ruthenium(POCOP) hydridochloride complex and studied via low temperature NMR under D_2. Additionally, an unusual 14-electron ruthenium(POCOP) species was isolated and studied by NMR. Preliminary catalytic screening for C-C bond coupling, C-H activation and ketone hydrogenation reactions was conducted.

5.0 Future Work

Additional work is needed for characterization of **60** in the form of crystals for structural analysis. Also, **60** should be thoroughly studied in catalysis involving activation and bond cleavage of strong σ-bonds (C-H, N-H).

Furthermore, the preparation of osmium and rhodium POCOP pincer-ligated complexes **64** and **65** should be investigated. It should be very interesting comparing their structural and electronic properties to analogous POCOP ruthenium and iridium complexes (Chart 32). Once prepared, these complexes should be catalytically screened for C-C bond coupling, C-H, and N-H bond activation reactions.

Chart 33

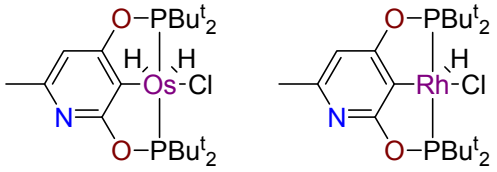

64 **65**

As demonstrated by Goldman and Liu, the size of the flanking phosphorus group can be very influential on catalysis. They showed that more catalytically active metals are generated upon replacement of bulky *tert*-butyl groups with medium size isopropyl groups.[19] Consequently, the preparation of a new POCOP ligand containing di(isopropyl) phosphorus groups should be investigated. This new ligand should give rise to more active metal species (Chart 33).

Chart 34

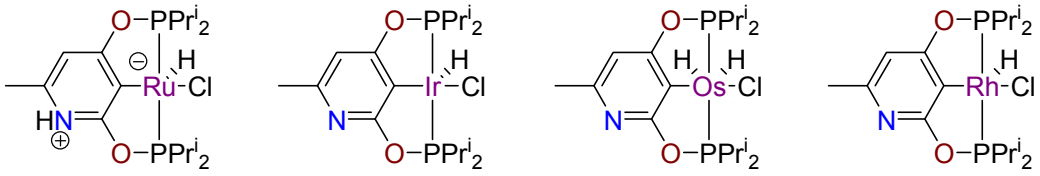

6.0 Experimental

General Comments

All room-temperature reactions were carried out under argon in a glovebox. When heating was required, the reaction mixture was transferred out of the box, attached to a manifold, and opened under Ar. Anhydrous deuterated and regular solvents were stored and used in the glovebox. NMR measurements were done on a Varian 300 MHz spectrometer. All solvents and reagents were purchased from Aldrich.

Computational Details

All molecular geometries were fully optimized using the MPW1PW91 functional implemented in Gaussian 03[34] which included modified Perdew-Wang exchange and Perdew-Wang 91 correlation.[35] The nature of all stationary points was verified by frequency calculations. The basis sets employed in this work included SDD (associated with ECP) for Ru, and Ir, 6-31g for the CH_3 groups of PBu^t_2, 6-311+g(d) for P and Cl, 6-31++g(d,p) for all other atoms.[36]

Pyridine-2,4-bis(di-*t*-butyl phosphinite)

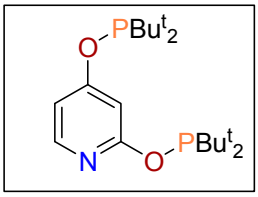

Pyridine-2,4-diol (2.00 g, 18.00 mmol) was combined with 7.48 g of di(*t*-butyl)chlorophosphine (41.40 mmol) and 5.47 g of triethylamine (54.00 mmol) in 25 mL of propionitrile. The reaction mixture was stirred and heated to 90 °C for 20 h yielding a pale yellow solution containing white precipitate. After cooling the reaction mixture to room temperature, the solution was filtered and the filtrate was evaporated under reduced

pressure yielding a pale yellow solid. The product was extracted from the solid in 3 x 10 mL of diethylether, followed by evaporation of the solvent under vacuum yielding 6.97 g (97 %) of the phosphinite as a pale yellow solid. ^{1}H {^{31}P} NMR (C_6D_6): δ 8.00 (d, $^{3}J_{HH}$ = 4.5 Hz, 1H, pyridyl-*H*), 7.02 (s, 1H, pyridyl-*H*), 6.67 (m, 1H, pyridyl-*H*), 1.18 (s, 18H, C*H*$_3$), 0.98 (s, 18H, C*H*$_3$). ^{31}P NMR (C_6D_6): δ 155.17, 154.17.

Pyridine-2,4-bis(di-*t*-butyl phosphine-borane)

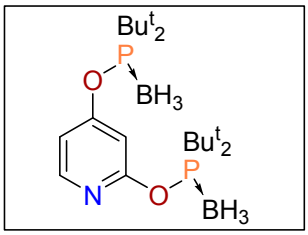

Pyridine-2,4-bis(di-*t*-butyl phosphinite) (0.50 g, 1.25 mmol) and 6.74 g of 1 M BH_3/THF (7.51 mmol) was added to a 20 mL vial and swirled until the solid material dissolved. Then the vial was stored in a freezer at -15 °C for 5 h, followed by removal of the solvent and drying under vacuum, yielding 0.43 g (81 %) of the product as a white solid. ^{1}H NMR (C_6D_6): δ 7.95 (d, $^{3}J_{HH}$ = 5.7 Hz, 1H, pyridyl-*H*), 7.47 (s, 1H, pyridyl-*H*), 6.76 (m, 1H, pyridyl-*H*), 1.31 (d, $^{3}J_{HP}$ = 13.5 Hz, 18H, C*H*$_3$), 1.11 (d, $^{3}J_{HH}$ = 13.5 Hz, 18H, C*H*$_3$). ^{31}P NMR (C_6D_6): δ 157.28 (bm), 155.79 (bm).

Pyridine-2,4-bis(di-*t*-butyl phosphinate)

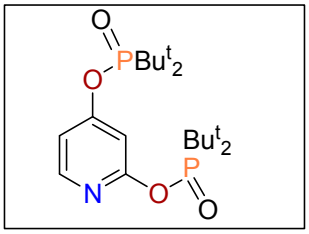

Pyridine-2,4-bis(di-*t*-butyl phosphinite) (0.10 g, 0.26 mmol), and 0.07 g of 10.4 M hydrogen peroxide (0.52 mmol) was combined in a flask containing 3 mL of THF. The

mixture was stirred at room temperature for 1 h, followed by evaporation of THF and drying. This yielded 0.11 g (95%) of the product as white solid. ^{1}H NMR (CD_2Cl_2): δ 8.10 (d, $^{3}J_{HH}$ = 5.7 Hz, 1H, pyridyl-*H*), 7.22 (m, 1H, pyridyl-*H*), 7.19 (s, 1H, pyridyl-*H*), 1.33 (d, $^{3}J_{HP}$ = 7.8 Hz, 18H, C*H*$_3$), 1.28 (d, $^{3}J_{HP}$ = 7.8 Hz, 18H, C*H*$_3$). ^{31}P NMR (CD_2Cl_2): δ 71.43, 68.74.

Pyridine-2,4-bis(di-*t*-butyl phosphinothioate)

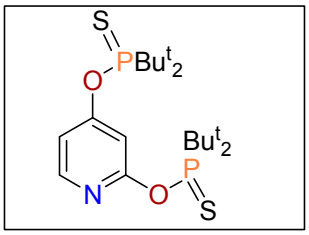

A flask containing pyridine-2,4-bis(di-*t*-butyl phosphinite) (1.00 g, 2.50 mmol), and 0.16 g of sulfur (0.06 mmol) in 10 mL of THF was stirred and refluxed for 4 h. After the solution was cooled to room temperature, THF was evaporated under vacuum. This yielded 1.10 g (95%) of the sulfide as white solid. ^{1}H {^{31}P}NMR (toluene-d8): δ 7.96 (d, $^{3}J_{HH}$ = 5.4 Hz, 1H, pyridyl-*H*), 7.53 (s, 1H, pyridyl-*H*), 6.90 (m, 1H, pyridyl-*H*), 1.36 (s, 18H, C*H*$_3$), 1.20 (s, 18H, C*H*$_3$). ^{31}P NMR (C_6D_6): δ 131.19, 130.29.

Pyridine-2,4-bis(di-*t*-butyl phosphinoselenoate)

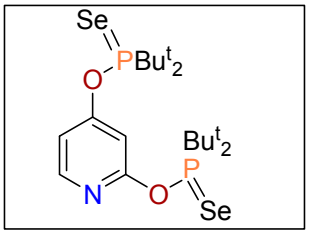

A flask containing pyridine-2,4-bis(di-*t*-butyl phosphinite) (0.22 g, 0.55 mmol), and 0.09 g of selenium (1.14 mmol) in 4 mL of toluene was stirred and heated to 80 °C for 4 h.

After the solution was cooled to room temperature, toluene was evaporated under vacuum. This yielded 0.27 g (89%) of the selenide as white solid.

1-Methylpyridinium-2,4-bis(di-*t*-butyl phosphine-borane) Tetrafluoroborate

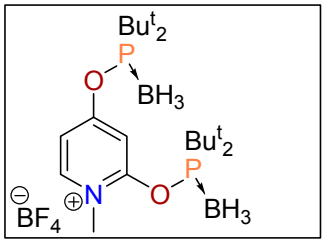

Pyridine-2,4-bis(di-*t*-butyl phosphine-borane) (0.39 g, 0.91 mmol) and 0.13 g trimethyloxonium tetrafluoroborate (0.88 mmol) were combined in a flask containing 3 mL of dichloromethane. The reaction mixture was stirred for 4 h at room temperature followed by evaporation of dichloromethane under vacuum. This yielded 0.47 g (98 %) of the product as white solid. ^{1}H NMR (CD_2Cl_2): δ 8.53 (d, $^{3}J_{HH}$ = 7.5 Hz, 1H, pyridyl-*H*), 7.97 (s, 1H, pyridyl-*H*), 7.47 (m, 1H, pyridyl-*H*), 4.14 (s, 3H, N-CH_3), 1.38 (m, 36H, CH_3).^{31}P NMR (CD_2Cl_2): 182.47 (bs), 171.69 (bd).

1-Methylpyridinium-2,4-bis(di-*t*-butyl phosphinate) Tetrafluoroborate

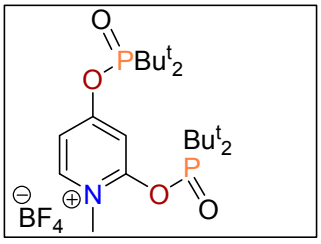

Pyridine-2,4-bis(di-*t*-butyl phosphinate) (0.11 g, 0.25 mmol) and 0.04 g trimethyloxonium tetrafluoroborate (0.24 mmol) were combined in a flask containing 3 mL of dichloromethane. The reaction mixture was stirred for 4 h at room temperature followed by evaporation of dichloromethane under vacuum. This yielded 0.11 g (86 %) of the product as white solid. ^{1}H NMR (CD_2Cl_2): δ 8.48 (d, $^{3}J_{HH}$ = 7.2 Hz, 1H, pyridyl-

H), 8.44 (s, 1H, pyridyl-*H*), 7.59 (m, 1H, pyridyl-*H*), 4.09 (s, 3H, N-CH_3), 1.35 (m, 36H, CH_3).^{31}P NMR (CD_2Cl_2): 84.89, 80.15.

1-Methylpyridinium-2,4-bis(di-*t*-butyl phosphinothioate) Tetrafluoroborate

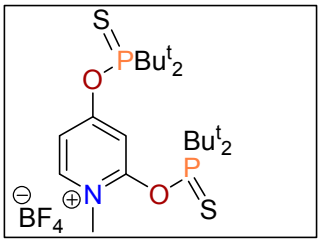

Pyridine-2,4-bis(di-*t*-butyl phosphinothioate) (0.12 g, 0.26 mmol) and 0.04 g trimethyloxonium tetrafluoroborate (0.27 mmol) were combined in a flask containing 5 mL of dichloromethane. The reaction mixture was stirred for 4 h at room temperature followed by evaporation of dichloromethane under vacuum. This yielded 0.14 g (98 %) of the product as white solid. ^{1}H NMR (CD_2Cl_2): δ 8.77 (d, $^3J_{HH}$ = 2.7 Hz, 1H, pyridyl-*H*), 8.56 (d, $^3J_{HH}$ = 7.2 Hz, 1H, pyridyl-*H*), 7.40 (m, 1H, pyridyl-*H*), 4.13 (s, 3H, N-C*H*3), 1.45 (m, 36H, CH_3). ^{31}P NMR (CD_2Cl_2): δ 150.47, 142.52.

6-Methylpyridine-2,4-bis(di-*t*-butyl phosphinite) (POCOP)

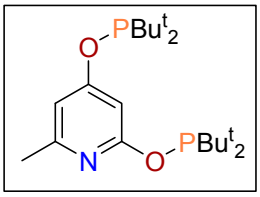

6-Methylpyridine-2,4-diol (2.00 g, 15.85 mmol) was combined with 6.64 g (36.75 mmol) of di(*t*-butyl)chlorophosphine in 30 mL of propionitrile. The mixture was stirred for 5 minutes at room temperature followed by addition of 4.85 g (47.91 mmol) of triethylamine. The mixture was stirred and refluxed for 21 h yielding a yellow solution containing a white crystalline precipitate. After cooling the reaction mixture to room

temperature for 1 hour, the mixture was filtered and the yellow filtrate collected was evaporated under reduced pressure. Then the product was extracted from the light yellow solid material in 3 x 10 mL of diethylether followed by evaporation of the solvent under reduced pressure. The resulting pale yellow solid was dried under vacuum yielding 6.01 g (91%) of the phosphinite. ^{1}H NMR (C_6D_6): δ 7.00 (s, 1H, pyridyl-*H*), 6.73 (s, 1H, pyridyl-*H*), 2.31 (s, 3H, pyridyl-C*H*$_3$), 1.22 (d, $^{3}J_{HP}$ = 11.4 Hz, 18H, C*H*$_3$), 1.06 (d, $^{3}J_{HP}$ = 12.0 Hz, 18H, C*H*$_3$). ^{13}C NMR (C_6D_6): δ 169.65 (d, $^{2}J_{CP}$ = 10.4 Hz, pyridyl-*C*), 166.92 (d, $^{2}J_{CP}$ = 7.4 Hz, pyridyl-*C*), 158.97 (s, pyridyl-*C*), 108.58 (d, $^{3}J_{CP}$ = 10.7 Hz, pyridyl-*C*), 98.56 (dd, $^{3}J_{CP}$ = 5.1, 13.1 Hz, pyridyl-*C*), 35.99 (d, $^{1}J_{CP}$ = 26.6 Hz, *C*(CH$_3$)$_3$), 35.95 (d, $^{1}J_{CP}$ = 28.6 Hz, *C*(CH$_3$)$_3$), 28.15 (d, $^{2}J_{CP}$ = 16.1 Hz, C(*C*H$_3$)$_3$), 27.67 (d, $^{2}J_{CP}$ = 15.8 Hz, C(*C*H$_3$)$_3$), 24.707 (s, *C*H$_3$). ^{31}P NMR (C_6D_6): δ 153.80, 152.96.

[IrHCl(POCOP)]

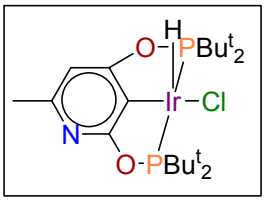

Toluene (30 mL) was added to a flask containing 0.74 g (1.78 mmol) of POCOP and 0.70 g (0.78 mmol) of [IrCl(COE)$_2$]$_2$ and the solution was stirred at room temperature for 10 minutes. The temperature was increased to 110 °C and stirred for an additional 24 h resulting in a deep red solution. Then the reaction mixture was cooled to room temperature followed by evaporation of the solvent under reduced pressure giving an orange/red color solid. The solid material was washed with 3 x 4.5 mL of hexane, then 3 x 3 mL of diethylether, followed by another 4.5 mL portion of hexane. After drying under vacuum, 0.87 g (87%) of [IrHCl(POCOP)] was obtained as an orange solid. ^{1}H NMR

(C_6D_6): δ 6.38 (s, 1H, pyridyl-*H*), 2.40 (s, 3H, pyridyl-CH_3), 1.25 (m, 36H, CH_3), -40.61 (t, $^2J_{HP}$ = 13.2, 26.1 Hz, 1H, Ir*H*). ^{13}C NMR (C_6D_6): δ 175.62 (dd, $^2J_{CP}$ = 9.8 Hz, $^3J_{CP}$ = 6.9 Hz, pyridyl-*C*), 174.76 (dd, $^2J_{CP}$ = 7.3 Hz, $^3J_{CP}$ = 4.9 Hz, pyridyl-*C*), 154.55 (s, pyridyl-*C*CH_3), 107.68 (m, Ir*C*), 103.02 (d, $^3J_{CP}$ = 10.2 Hz, pyridyl-*C*H), 43.29 (m, *C*$(CH_3)_3$), 39.82 (m, *C*$(CH_3)_3$), 27.89 (m, C(*C*$H_3)_3$), 24.48 (s, pyridyl-*C*H_3). ^{31}P NMR (C_6D_6): δ 183.47 (d, $^2J_{PP}$ = 357.0 Hz), 162.48 (d, $^2J_{PP}$ = 357.0 Hz).

[IrHCl(POCOP-NCH$_3$)]$^+$ BF$_4^-$

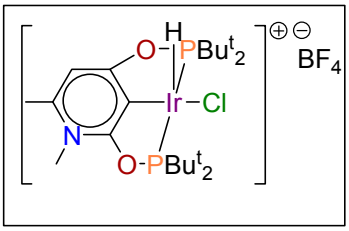

A flask was charged with 0.50 g (0.78 mmol) of [IrHCl(POCOP)], 0.12 g (0.78 mmol) of trimethyloxonium tetrafluoroborate and 15 mL of dichloromethane. The reaction flask was submerged in an ultrasonic bath for 2 hrs giving a dark orange solution. Dichloromethane was evaporated under vacuum resulting in an orange, sticky solid. The material was washed with 2 x 2mL of toluene and dried under vacuum yielding 0.54 g (93%) of [IrHCl(POCOP-NCH$_3$)]$^+$ BF$_4^-$ as a yellow solid. ^{1}H NMR (CD_2Cl_2): δ 6.92 (s, 1H, pyridyl-*H*), 4.06 (s, 3H, N-CH_3), 2.62 (s, 3H, pyridyl-CH_3), 1.43 (m, 36H, CH_3), -40.06 (t, $^2J_{HP}$ = 12.6, 25.5 Hz, 1H, Ir*H*). ^{13}C NMR (CD_2Cl_2): δ 177.70 (dd, $^2J_{CP}$ = 6.75 Hz, $^3J_{CP}$ = 5.48 Hz, pyridyl-*C*), 167.98 (dd, $^2J_{CP}$ = 9.9 Hz, $^3J_{CP}$ = 7.88 Hz, pyridyl-*C*), 149.23 (s, pyridyl-*C*CH_3), 113.96 (q, $^2J_{CP}$ = 3.60, 11.25 Hz, Ir*C*), 107.10 (dd, $^3J_{CP}$ = 2.4, 6.6 Hz, pyridyl-*C*H), 44.26 (m, *C*$(CH_3)_3$), 41.03 (m, *C*$(CH_3)_3$), 37.85 (s, N*C*H_3), 27.66 (m, *C*H_3), 20.93 (s, pyridyl-*C*H_3). ^{31}P NMR (CD_2Cl_2): δ 193.47 (d, $^2J_{PP}$ = 352.4 Hz), 193.36 (d, $^2J_{PP}$ = 352.4 Hz).

[IrCl(POCOP-NCH$_3$)]

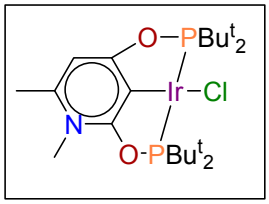

A solution containing 1.12 g (1.50 mmol) of [IrHCl(POCOP-NCH$_3$)]BF_4 and 15 mL of THF was prepared and treated with 0.46 g (4.50 mmol) of triethylamine yielding a dark red solution. The solution was stirred at room temperature for 2 h followed by evaporation of THF under reduced pressure which resulted in a sticky orange/red solid. The product was extracted in 4 x 5 mL of toluene and the solution was concentrated by half and stored in a freezer for 24 h. Afterwards the solid precipitate was filtered and the filtrate was evaporated under vacuum giving a red solid. The material was washed with 3 x 3 mL of hexane and dried under vacuum yielding 0.430 g (44%) of [IrCl(POCOP-NCH$_3$)] as a dark orange solid. ^{1}H NMR (THF-d8): δ 6.39 (s, 1H, pyridyl-*H*), 3.87 (s, 3H, NC*H*$_3$), 1.77 (s, 3H, pyridyl-C*H*$_3$), 1.40 (m, 36H, C*H*$_3$). ^{13}C NMR (THF-d8): δ 175.66 (m, pyridyl-*C*CH$_3$), 168.05 (m, pyridyl-*C*), 132.04 (s, pyridyl-*C*CH$_3$), 130.83 (m, pyridyl-*C*H), 104.65 (m, Ir*C*), 41.04 (m, *C*(CH$_3$)$_3$), 35.16 (s, NCH$_3$), 27.63 (m, *C*H$_3$), 19.84 (s, pyridyl-*C*H$_3$). ^{31}P NMR (THF-d8): δ 193.76 (d, $^2J_{PP}$ = 418.1 Hz), 193.60 (d, $^2J_{PP}$ = 418.1 Hz).

[RuHCl(POCOP-NH)]

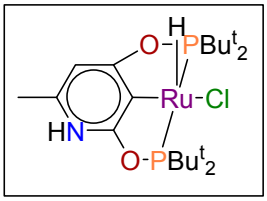

POCOP (0.90 g, 2.18 mmol) was combined with 0.56 g (0.91 mmol) of $[RuCl_2(p\text{-cymene})]_2$ in 30 mL of 2-propanol. Then 0.58 g (5.44 mmol) of 2,6-lutidine was added and the mixture was stirred for 30 minutes at room temperature. The flask was opened to vacuum for 1 min, then refilled with H_2(g) and heated to 85 °C for an additional 20 h giving a dark red solution. After cooling the mixture to room temperature, 2-propanol was removed under reduced pressure giving a sticky red solid. Next, the solid was washed with 4 x 5 mL H_2O, then the product extracted in 4 x 5 mL toluene. The 20 mL solution was concentrated to 5 mL and stored in the freezer for 24 h. Following crystallization, the solvent was removed through decantation and the precipitate was washed with 3 x 3 mL of hexane and dried under vacuum giving 0.51 g (51%) of the product [RuHCl(POCOP-NH)] as a red solid. ^{1}H NMR (THF-d^8): δ 12.38 (s, 1 H, pyridyl-N*H*), 6.31 (s, 1 H, pyridyl-*H*), 2.59 (s, 3 H, pyridyl-CH_3), 1.31 (m, 36 H, CH_3), -30.42 (t, $^2J_{HP}$ = 21.6, 43.2 Hz, 1 H, Ru*H*). ^{13}C NMR (THF-d^8): δ 181.24 (dd, $^2J_{CP}$ = 8.29, 12.06 Hz, py-*C*), 168.37 (dd, $^2J_{CP}$ = 8.29, 19.6 Hz, py-*C*), 138.61 (s, py-*C*), 133.1 (s, py-*C*), 101.62 (d, $^3J_{CP}$ = 9.43 Hz, py-*C*H), 42.52 (d, J_{CP} = 4.9 Hz, *C*(CH$_3$)$_3$), 42.29 (m, *C*(CH$_3$)$_3$), 40.06 (d, J_{CP} = 2.71 Hz, *C*(CH$_3$)$_3$), 39.99 (d, J_{CP} = 2.87 Hz, *C*(CH$_3$)$_3$), 39.76 (d, J_{CP} = 5.50 Hz, *C*(CH$_3$)$_3$), 39.70 (d, J_{CP} = 4.98 Hz, *C*(CH$_3$)$_3$), 29.00 (m, *C*H$_3$), 28.44 (d, J_{CP} = 7.31 Hz, *C*H$_3$), 28.35 (d, J_{CP} = 6.33 Hz, *C*H$_3$), 18.76 (s, *C*H$_3$). ^{31}P NMR (THF-d^8): δ 218.97 (d, $^2J_{PP}$ = 350.9 Hz), 213.87 (d, $^2J_{PP}$ = 350.9 Hz).

[RuH(POCOP)]

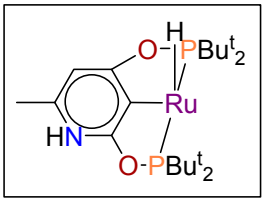

0.20 g (0.36 mmol) of [RuHCl(POCOP-NH)] was combined with 0.04 g (0.36 mmol) of potassium *tert*-butoxide in 10 mL of 2-propanol and stirred for 1 h at room temperature giving a deep purple solution. Subsequently, 2-propanol was removed under reduced pressure and the dark purple solid was dried for 2 h. The product was extracted in 3 x 3 mL of toluene followed by evaporation of the solvent under vacuum yielding 0.19 g of [RuH(POCOP)] as a shinny deep purple solid. An NMR sample prepared in hydrocarbon solvent C_6D_6 showed evidence of several products present. However, the product cleanly forms solvent-complexes with THF and acetonitrile, indicating the product had not undergone any decomposition.

[$RuCl_2$(p-cymene)]$_2$

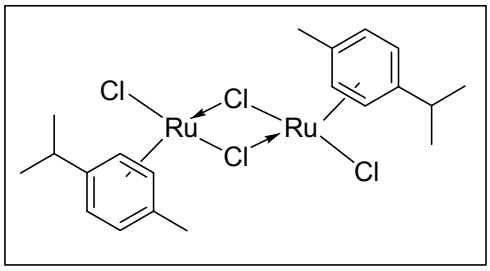

A 500 mL Schlenk flask was charged with 5.00 g (19.10 mmol) of ruthenium trichloride and 200 mL of 2-propanol. The mixture was degassed and refilled with argon and stirred for 5 min. This was followed by addition of 25 mL of R-α-phellandrene under a stream of argon. The mixture was stirred at 95 °C for 5 h producing a dark green solution. Then 2.10 g (19.60 mmol) of 2, 6-lutidine was added and the mixture was stirred at 95 °C for

15 h giving a dark red solution. The flask was left at room temperature for 1 hour followed by 3 h in the freezer (-15 °C). Dark red solid material settled in the flask and was later filtered (in air), washed with 3 x 10 mL ethanol and dried under vacuum. This yielded 5.17 g (88%) of $[RuCl_2(p\text{-cymene})]_2$ as a dark brown solid.

$[IrCl(COE)_2]_2$

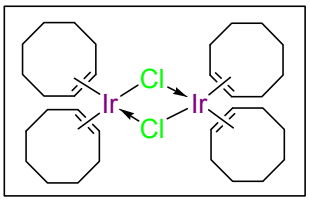

Synthesis of $[IrCl(COE)_2]_2$ was previously described in the literature, however we present a modified preparation that gives moderately better yields. A mixture of 2-propanol/degassed water (50 mL/150 mL) was added to 6.00 g (17.00 mmol) of $IrCl_3 \bullet 3H_2O$. Then 20 mL of cyclooctene was added and the mixture was stirred vigorously and refluxed at 100 °C for 24 h. After cooling at room temperature, the solution was removed by decantation and the orange oily residue was triturated in 30 mL of ethanol. This gave an orange suspension which was filtered and washed with 2 x 6 mL of ethanol and dried under vacuum. This gave 5.24 g (69%) of $[IrCl(COE)_2]_2$ as an orange solid.

References

[1] Wanzlick, H. W. *Angew. Chem.* **1961**, 73, 493.

[2] Arduengo, A. J., III; Harlow, R. L.; Kline, M. *J. Am. Chem. Soc*. **1991**, 113, 361.

[3] Sommer, W. J.; Weck, M. *Coord. Chem. Rev.* **2007**, 251, 860.

[4] Chianese, A. R.; Kovcevic, A.; Zeglis, B. M.; Faller, J. W.; Crabtree, R. H. *Organometallics*. **2004**, 23, 2461.

[5] (a) Huang, J.; Stevens, E. D.; Nolan, S. P.; Peterson, J. L. *J. Am. Chem. Soc.* **1999**, 121, 2674. (b) Scholl, M.; Trnka, T. M.; Morgan, J. P.; Grubbs, R. H. *Tetrahedron Lett.* **1999**, 40, 2247. (c) Jafarpour, L.; Nolan, S. P. *Organometallics.* **2000**, 19, 2055.

[6] Scholl, M.; Ding, S.; Lee, C. W.; Grubbs, R. H. *Org. Lett.* **1999**, 1, 953.

[7] Schrock, R. R.; Murdzeck, J; Bazan, G. C.; Robbins, J.; Dimare, M.; O'Regan, M. *J. Am. Chem. Soc.* **1990**, 112, 3875.

[8] (a) Schwab, P.; France, M. B.; Ziller, J. W. *Angew. Chem.* **1995**, 34, 2039. (b) Schwab, P.; Grubbs, R. H.; Ziller, R. H. *J. Am. Chem. Soc.* **1996**, 118, 100.

[9] (a) Diez-Gonzalez, S.; Nolan, S. P. *Coord. Chem. Rev.* **2007**, 251, 874. (b) Cavallo, L. *J. Am. Chem. Soc.* **2002**, 124, 8965.

[10] Grudemann, S.; Kovacevic, A.; Albrecht, M.; Faller, J. W.; Crabtree, R. H. *J. Am. Chem. Soc.* **2002**, 124, 10473.

[11] Castan, P.; Dahan, F.; Wimmer, S. *J. Chem. Soc. Dalton. Trans.* **1990**, 2971.

[12] Castan, P.; Jaud, J.; Wimmer, S.; Wimmer, F. L. *J. Chem. Soc. Dalton. Trans.* **1991**, 1155.

[13] Newman, C. P.;Clarkson, G. J.; Alcock, N. W.; Rouke, J. P. *J. Chem. Soc. Dalton Trans*. **2006**, 3321.

[14] (a) Schneider, S. K.; Gerrit, R. J.; Loschen, C.; Raubenheimer, H. G.; Frenking, G.; Herrmann, W. A. *J. Chem. Soc. Dalton Trans.* **2006**, 1126. (b) Schneider, S. K.; Roembke, P.; Julius, G. R.; Raubenheimer, H. G, Herrmann, W. A. *Adv. Synth. Catal.* **2006**, 348, 1862. (c) Meyer, W. H.; Deetlefs, M.; Pohlmann, M.; Scholz, R.; Esterhuysen, M. W.; Julius, G. R.; Raubenheimer, H. G. *J. Chem. Soc. Dalton Trans.* **2004**, 413.

[15] Albrecht, M.; van Koten, G. *Angew. Chem. Int. Ed.* **2001**, 40, 3750.

[16] Gupta, M.; Hagen, C.; Flesher, R. J.; Kaska, W. C.; Jensen, C. M. *Chem. Commun.* **1996**, 2083.

[17] Jensen, C. M.; *Chem. Commun.* **1999**, 2443.

[18] Göttker-Schnetmann, I.; White, P.; Brookhart, M. *J. Am. Chem. Soc.* **2004**, 126, 1804.

[19] Liu, F.; Goldman, A. S. *Chem. Commun.* **1999**, 655.

[20] (a) Goldman. A. S.; Roy, A. H., Huang, Z.; Ahuja, R.; Schinski, W.; Brookhart, M. *Science*. **2006**, 312, 257. (b) Huang, Z.; Brookhart, M.; Golman, A. S.; Kundu, S.; Ray, A., Scott, S. L.; Vicente, B. C. *adv. Synth. Catal.* **2009**, 351, 188.

[21] (a) Zhang, J.; Leitus, G.; Ben-David, Y.; Milstein, D. *J. Am. Chem. Soc.* **2005**, 127, 10840. (b) Zhang, J.; Gandelman, M.; Shimon, L. J. W.; Milstein, D. *J. Chem. Soc. Dalton Trans.* **2007**, 107. (c) Gunanathan, C.; Ben-David, Y.; Milstein, D. *Science*. **2007**, 317, 790. (d) Zhang, J.; Leitus, G.; Ben-David, Y.; Milstein, D. *Angew Chem. Int. Ed.* **2006**, 45, 1113.

[22] Imamoto, T.; Oshiki, T.; Onozawa, T.; Kusumoto, T.; Sato, K. *J. Am. Chem. Soc.* **1990**, 112, 5244.

[23] (a) Kottsieper, K. W.; Stelzer, O.; Wasserscheid, P. *J. Mol. Cat. A.* ***2001****, 175, 285.* (b) Steinberger, H. U.; Ziemer, B.; Meisel, M. *Acta Cryst.* **2001**, 57, 323. (c) Aguiar, A. M.; Smiley Irelan, J. R. *J. Org. Chem.* **1969**, 34, 11, 3349.

[24] Haynes, R. K.; Freeman, R. N.; Mitchell, C. R.; Vonwiller, S. C. *J. Org. Chem.* **1994**, 59, 2919.

[25] Romeo, R.; Wozniak, L. A., Chatgilialoglu, C. *Tetrahedron Lett.* **2000**, 41, 9899.

[26] Kuznetsov, V. F.; Abdur-Rashid, K.; Lough, A.; Gusev, D. G. *J. Am. Chem. Soc.* **2006**, *128*, 14388.

[27] Herde, J. L.; Lambert, J. C.; Senoff, C. V. *Inorg. Synth.* **1974**, 15, 18.

[28] (a) Kaesz, H. D.; Saillant, R. B. *Chem. Rev.* **1972**, 72, 3, 231. (b) McGrady, G. S.; Guilera, G. *Chem. Soc. Rev.* **2003**, 32, 383.

[29] Burk, M. J.; McGrath, M. P.; Wheeler, R.; Crabtree, R. H. *J. Am. Chem. Soc.* **1988**, 110, 5034.

[30] Gusev, D. G.; Dolgushin, F. M.; Antipin, M. Y. *Organometallics*. **2000**, 19, 3429.

[31] Ohff, M.; Ohff, A.; van der Boom, M. E.; Milstein, D. *J. Am. Chem. Soc.* **1997**, 119, 11687.

[32] Morales-Morales, D.; Redón, R.; Yung, C.; Jensen, C. M. *Chem. Commun.* **2000**, 1619.

[33] Kubas, G. J.; Ryan, R. R.; Swanson, B. I.; Vergamini, P. J.; Wasserman, H. J. *J. Am. Chem. Soc*. **1984**, 106, 451.

[34] Gaussian 03, Revision B.05, Frisch, M. J.; Trucks, G. W.; Schlegel, H. B.; Scuseria, G. E.; Robb, M. A.; Cheeseman, J. R.; Montgomery, Jr., J. A.; Vreven, T.; Kudin, K. N.; Burant, J. C.; Millam, J. M.; Iyengar, S. S.; Tomasi, J.; Barone, V.; Mennucci, B.; Cossi, M.; Scalmani, G.; Rega, N.; Petersson, G. A.; Nakatsuji, H.; Hada, M.; Ehara, M.;

Toyota, K.; Fukuda, R.; Hasegawa, J.; Ishida, M.; Nakajima, T.; Honda, Y.; Kitao, O.; Nakai, H.; Klene, M.; Li, X.; Knox, J. E.; Hratchian, H. P.; Cross, J. B.; Bakken, V.; Adamo, C.; Jaramillo, J.; Gomperts, R.; Stratmann, R. E.; Yazyev, O.; Austin, A. J.; Cammi, R.; Pomelli, C.; Ochterski, J. W.; Ayala, P. Y.; Morokuma, K.; Voth, G. A.; Salvador, P.; Dannenberg, J. J.; Zakrzewski, V. G.; Dapprich, S.; Daniels, A. D.; Strain, M. C.; Farkas, O.; Malick, D. K.; Rabuck, A. D.; Raghavachari, K.; Foresman, J. B.; Ortiz, J. V.; Cui, Q.; Baboul, A. G.; Clifford, S.; Cioslowski, J.; Stefanov, B. B.; Liu, G.; Liashenko, A.; Piskorz, P.; Komaromi, I.; Martin, R. L.; Fox, D. J.; Keith, T.; Al-Laham, M. A.; Peng, C. Y.; Nanayakkara, A.; Challacombe, M.; Gill, P. M. W.; Johnson, B.; Chen, W.; Wong, M. W.; Gonzalez, C.; and Pople, J. A.; Gaussian, Inc., Wallingford CT, **2004**.

[35] (a) Adamo, C.; Barone V. *J. Chem. Phys.* **1998**, *108*, 664. (b) Perdew, J. P.; Burke, K.; Wang, Y., *Phys. Rev. B* **1996**, *54*, 16533. (c) Burke K.; Perdew, J. P.; Wang, Y., in *Electronic Density Functional Theory: Recent Progress and New Directions*, Ed. Dobson, J. F.; Vignale, G.; Das, M. P., Plenum 1998.

[36] For more information about basis sets implemented in Gaussian 03 and references see Frish, A.; Frish, M. J.; Trucks, G. W. *Gaussian 03 User's Reference*, Gaussian, Inc., Pittsburgh PA, 2003. The basis sets are also available from the Extensible Computational Chemistry Environment Basis Set Database, which is developed and distributed by the Molecular Science Computing Facility, Environmental and Molecular Sciences Laboratory, which is part of the Pacific Northwest Laboratory, P.O. Box 999, Richland, Washington 99352, USA (www.emsl.pnl.gov/forms/basisform.html).